Assessing the impacts of assimilating satellite SST in addition to along-track SLA into a HYCOM of the Agulhas System

Minor Dissertation presented in partial fulfilment of the requirements for the degree of Master of Science

In the Department of Oceanography

University of Cape Town

August 2017

Supervisors: Dr B. Backeberg & A/Prof M. Rouault

UNIVERSITY OF CAPE TOWN

IYUNIVESITHI YASEKAPA • UNIVERSITEIT VAN KAAPSTAD

Declaration

I know that plagiarism is wrong. Plagiarism is to use another's work and pretend that it is one's own.

I have used the Harvard convention for citation and referencing. Each contribution to, and quotation in, this dissertation, from the work(s) of other people has been attributed, and has been cited and referenced.

This dissertation is my own work.

I have not allowed, and will not allow, anyone to copy my work with the intention of passing it off as his or her own work.

Signed by candidate

Signed

Tharone Rapeti

August 2017

Acknowledgements

Thanks to my supervisors for providing me with the necessary support, and guidance when needed. Thanks to the NRF and ACCESS for providing me with the funding required to pursue my Masters, your assistance is truly appreciated. To the Department of Oceanography, thank you to all for the great year that passed. Huge thanks to my classmates, for always being around to help, talk or just being there, could not ask for better friends. Thanks to my brother, Desigan, for always being available to take time off and hang out. Shan, I owe you some huge thanks for always helping me with my editing, and for all the advice you've given to me. Finally, a special thanks to my parents and sister, without you'll I would not have gotten this far, I owe you'll everything. And thank you to any others who have helped along the way who I have not mentioned, each one of you have contributed towards my progress.

Assessing the impacts of assimilating satellite SST in addition to along-track SLA into a HYCOM of the Agulhas System

Abstract

The greater Agulhas Current System, is considered to be the largest western boundary current in the Southern Hemisphere, with only the Gulf Stream, and possibly the Kuroshio, considered to be larger globally (Bryden et al., 2005). The Current System is a crucial factor for determining the mean state and variability of the regional marine environment, resources and ecosystems in the region, regional weather, as well as the global climate on a broad range of temporal and spatial scales. Due to an absence of a coherent *in situ* and satellite-based observing system in the area, modelling and data assimilation techniques are utilised. These both further the quantitative understanding of the ocean dynamics as well as providing better forecasts of this complicated western boundary current system.

In this study, we compare two assimilation experiments using the Ensemble Optimal Interpolation (EnOI) data assimilation scheme in a regional implementation of the Hybrid Coordinate Ocean Model (HYCOM). In the first experiment, we assimilate along-track satellite sea level anomaly (SLA) data only, and in the second experiment we assimilate both along-track sea level anomaly (SLA) as well as satellite sea surface temperature (SST) data. The objectives of the study are to investigate the impacts of assimilating SST along with SLA into the regional HYCOM model, with the hopes of improving the model performance. The long term aim of this experiment is to develop a regional ocean prediction system.

The additional assimilation of SST along with SLA into the HYCOM model, has improved upon the representation of the SST field across the region by reducing the error. However, with regards to velocity, surface eddy kinetic energies (EKE), as well as subsurface velocities, the updated SST model shows less improvement. A velocity bias can be seen as the reason for underperformance in these aspects. The model still struggles to recreate subsurface water masses, underestimating salinity in the upper 500 m; assimilating T/S profiles in the future could improve on this. The assimilation of SST has improved upon the SST-SSH correlation in the model, as well as the spatial distribution and accuracy.

The assimilation of SST along with SLA has had many positive impacts, with unfortunately, a few negatives. The shortcomings of the numerical model will have to be improved upon and additional assimilation variables should be tested in further studies, to provide a solid forecasting system.

Table of Contents

Declaration ..... **i**

Acknowledgements ..... **ii**

Abstract ..... **iii**

Table of Contents ..... **v**

1. Introduction **6**

1.1. The Greater Agulhas Current System 9

1.1.1. Sources 10

1.1.2. Northern Agulhas Current 10

1.1.3. Southern Agulhas Current 12

1.1.4. Agulhas Current Transport 12

1.1.5. The Agulhas Retroflection 13

1.1.6. The Agulhas Return Current 14

1.1.7. Agulhas Rings 15

2. Data Assimilation System **17**

2.1.1. Browning and Kriess: Initialization of the Shallow Water Equations 21

2.1.2. Efficient and accurate bulk parameterizations of air-sea fluxes for use in general circulation models 22

2.2. Ensemble Optimal Interpolation 22

3. Observations **26**

3.1. Satellite Altimetry Data 26

3.2. Sea Surface Temperature Data 27

3.3. Drifter data 27

3.4. Argo floats 28

4. Results **29**

4.1. Surface and Subsurface Velocities 29

4.1.1. Surface Velocities 29

4.1.2. Subsurface velocities 37

4.2. Surface Eddy Kinetic Energies 38

4.3. Sea Surface Temperatures 42

4.4. T/S profiles 48

5. Summary and Outlook **50**

6. References **53**

1. Introduction

Considered one of the world's most dynamic ocean current regions, the Agulhas Current system, has a vital role in the resources and ecosystem of its marine environment, as well as on the local weather and global climate (Lutjeharms, 2006). The Agulhas Current proper is a western boundary current, one of the largest globally (Bryden et al., 2005), which flows poleward along the east coast of South Africa, and forms the closure of the South Indian subtropical gyre (Lutjeharms and Ansorge, 2001). The current closely follows the continental shelf until it reaches the southern tip of the African continental shelf, where it loops back onto itself and flows east, back into the Indian Ocean as the Agulhas Return Current (Lutjeharms and Ansorge, 2001). It is at this looping point, known as the Agulhas Retroflection, where there are high levels of mesoscale activity, with the formation and shedding of Agulhas Rings, anticyclonic eddies, and filaments into the South Atlantic (Lutjeharms and van Ballegooyen, 1988; (Lutjeharms and Gordon, 1987). The shedding of these rings and filaments play a crucial role in the mass exchange between the Indian and Atlantic Oceans (Biastoch et al., 2009). These rings and filaments contain warm and salty water from the Agulhas Region and transport it into the South Atlantic, a process known as Agulhas Leakage (de Ruijter, 1981). This leakage plays a big role in the Atlantic Meridional Overturning Circulation (AMOC), an oceanic conveyor belt which redistributes heat from the Southern Hemisphere to the Northern Hemisphere, this has global implications on the oceans and their influence on the climate (Peeters et al., 2004; Biastoch et al., 2008; Beal et al., 2011).

A recent study by Rouault et al. (2009) indicated a warming trend within the Agulhas Retroflection region, on the decadal time scale, since the 1980s. Observations of satellite altimetry from 1993-2009 have also noted changes in the area, with intensified variability in mesoscale activity within the greater Agulhas region, as well as in the retroflection region (Backeberg et al., 2012) having been identified. This increased mesoscale variability is made evident by the noticeable accelerated propagation of eddies in the Mozambique Channel, south of Madagascar, and within the retroflection region (Backeberg et al., 2012). It has also been hypothesised that Agulhas leakage has been increasing over that past few decades, supplying more salt rich water to the AMOC, and possibly having the ability to counteract the North Atlantic freshening, resulting from the melting ice-sheets and glaciers due to the anthropogenic warming of the global climate (Biastoch et al., 2008). A lack of data within the region hinders our ability to assess the true extent of the Agulhas Leakage, as well as its impacts on the global ocean circulation.

With all these changes being observed in the Agulhas Region, noting its importance to the global ocean climate, it is vital that the area be well understood and monitored. Being able to advance the predictability of the highly dynamic and variable features in the system, would also have benefit on

the industrial, commercial, and leisure sectors in the region south of Africa (Backeberg et al., 2014). A forecasting system in the region would be able to provide authorities with advanced warnings with regards to destructive oceanic events, saving lives and limiting damage to infrastructure in the shipping industry. Fisheries could utilise the system to predict the likely positioning of large fish populations; off-shore oil companies would be able to know where and when to deploy moorings and setup oil rigs; a forecasting system in the region would be invaluable. A comprehensive prediction system would also enable the improved monitoring of accidental pollutants, such as oil spills; in the event of plane crashes or ships sinking, the system could be used to track the flow of debris. Such a system would also enable environmental agencies to predict and monitor the formation and spread of harmful algal blooms.

However, the development of such a system is problematic due to the lack of a comprehensive *in situ* and satellite-based monitoring systems present in the Agulhas domain. Due to this lack of data, most studies in the area, and in particular those looking into Agulhas Leakage, have been largely reliant on numerical models of the system.

These numeric ocean models are widely used as tools for the better understanding of particular oceanic regions. However, in regions like the Agulhas which are known for their non-linear, highly variable mesoscale nature, numerical models are unable to provide a realistic representation of the systems (Biastoch et al., 2008). Most model simulations of the region, with some exceptions (Penven et al., 2010), produce a bias in the positioning of the Agulhas Retroflection, placing it too far east or further upstream (Lutjeharms and Webb, 1995), and with Agulhas Rings, the main source of leakage, following a consistent trajectory flowing into the South Atlantic Ocean (Barnier et al., 2006). This is not the case in reality where ring trajectory can vary (Morrow et al., 2004; Duncombe Rae, 1991; Duncombe Rae et al., 1996).

Using a global model developed by Thoppil et al., (2011), it was shown that merely improving the resolution of the model, from $1/12^{o}$ to $1/25^{o}$, did not improve the positioning of the retroflection or ring-shedding bias. Numerical models have also been proved to be particularly sensitive to adjustments in the numerical scheme; slight changes in precision (Backeberg et al., 2009) can deliver a completely different representation of the region being modelled. It has also been shown that changes to the conservation properties (Barnier et al., 2006) of the momentum advection scheme or by smoothing the topography, with the addition of a horizontal viscosity parameter, (Penven et al., 2006) would also produce a significantly altered representation of the Agulhas Current and the Retroflection. Differences between models, in a region with such a global ocean influence, is problematic as it can lead to wrong conclusions being drawn on mechanisms behind the warming

trend noted within the Retroflection (Rouault et al., 2009) and the leakage into the South Atlantic (van Sebille et al., 2009; Biastoch et al., 2009). Inaccuracies present in the initial state of the model further hinder the forecast ability of the model, up to the decadal time scale (Meehl et al., 2009). It is vital that the dynamics of the region are realistically represented and simulated in these ocean models, due to the potential global impact changes in the Agulhas region could be having on the global climate.

This is where data assimilation becomes useful. Assimilation aims to provide physically consistent 3-Dimensional estimates of the ocean state at a specific time. Reanalysis are 4-Dimensional reconstructions obtained by frequently assimilating available observations. Observations and numerical models both contain their own errors, observations are usually more accurate than models. If the true state of the ocean lies somewhere between the model and the observed data, one can attempt to approach the true ocean state, by combining both observed data and a numerical model, with their respective errors. By repeatedly assimilating *in situ* and observed data, models may then be adjusted/constrained to create a better representation of the ocean state thereby providing forecasts which would be more reliable and accurate. Through assimilation, we would be able to produce a regionally specific ocean based reanalysis product (Backeberg et al., 2014). This system would greatly assist in improving our knowledge of the dynamic and highly variable ocean circulations that exists in the Agulhas region.

Despite the availability of numerous global operational assimilation systems, systems which incorporate both *in situ* and satellite remotely sensed observations with a numerical model (e.g. MyOcean, Bluelink and FOAM (Forecast Ocean Assimilation Model), none have been developed specifically for the southern African regional ocean (Backeberg et al., 2014). There have been no regionally focused data assimilation experiments in the region since Evensen and van Leeuwen's work in 1996, until 2014, when Backeberg et al., (2014) developed a Hybrid Coordinate Ocean Model for the region which assimilated SLA using the EnOI.

This study follows up on the work done by Backeberg et al., (2014), where a regional data assimilation system covering the Agulhas region was presented. In that study, satellite altimeter along-track sea level anomaly (SLA) data, was assimilated into a HYCOM model (Bleck, 2002) using the Ensemble Optimal Interpolation (EnOI) data assimilation scheme. The HYCOM model had been shown to be able to reproduce a reasonable representation of the Agulhas Current system and the oceanographic features contained within (Backeberg et al., 2008, 2009), while the EnOI (Evensen, 2003; Oke et al., 2002) had been well utilised in regions with similar dynamics (Oke et al., 2005, 2007; Counillon and Bertino, 2009a, b; Xie et al., 2011; Srinivasan et al., 2011).

The study by Backeberg et al., (2014) highlighted the benefits of assimilating SLA into a free running numerical model. The assimilation outperformed the unassimilated numerical model in all but one of the areas tested, and it had some limitations. The assimilation system was unable to provide a better representation of surface velocities than those derived using satellite altimetry, AVISO (Archiving, Validation and Interpretation of Satellite Oceanographic Data); the assimilation process resulted in the degradation of the sea surface temperature (SST) field within the model, resulting in it being unable to accurately reproduce SST in the region; the numerical model was more accurate in this respect, containing less error. Errors within the numerical model fed into the assimilation as well; incorrect correlations of SSH and SST were reduced through assimilation but remained too high. Both the free numerical model and the assimilation were unable to accurately represent the Agulhas Return Current, either placing it too far to the south or not reproducing it at all.

This is where this study takes off; it looks to improve upon the successes of the previous assimilation experiment, while addressing the limitations as well. The same assimilation system was used; however, this study focuses on the impacts of assimilating SST along with SLA data, over the previous assimilation and the free running model. It is hoped that by assimilating SST into the model many of the previous shortfalls will be improved upon. The incorrect SSH-SST correlation, the degraded SST field, and the poor representation of the Agulhas Return Current are some of the shortfalls looking to be improved upon. The primary objective here being to eventually produce accurate regional forecasts, as well as more accurate regional reanalysis products.

1.1. The Greater Agulhas Current System

The Agulhas Current forms the western boundary of the South Indian Ocean subtropical gyre (Lutjeharms and Ansorge, 2001). This western boundary current flows south westward along the eastern coast of South Africa. The current closely follows the South African continental shelf, until it reaches the southern tip of the African continental shelf, the tip of the Agulhas Bank (Grundlingh, 1983). At this point the current turns around on itself, forming the Agulhas Retroflection. It is at this retroflection where the transfer of water between the South Atlantic and South Indian Ocean water occurs, through the shedding of Agulhas Rings (van Ballegooyen *et al*., 1994) and the leakage of Agulhas filaments (Lutjeharms and Cooper, 1996) into the South Atlantic. The water that is not transported into the South Atlantic then begins to flow back eastward, into the South Indian Ocean (Lutjeharms and Ansorge, 2001). This eastward flowing return current is known as the Agulhas Return Current (ARC) (Lutjeharms and Ansorge, 2001).

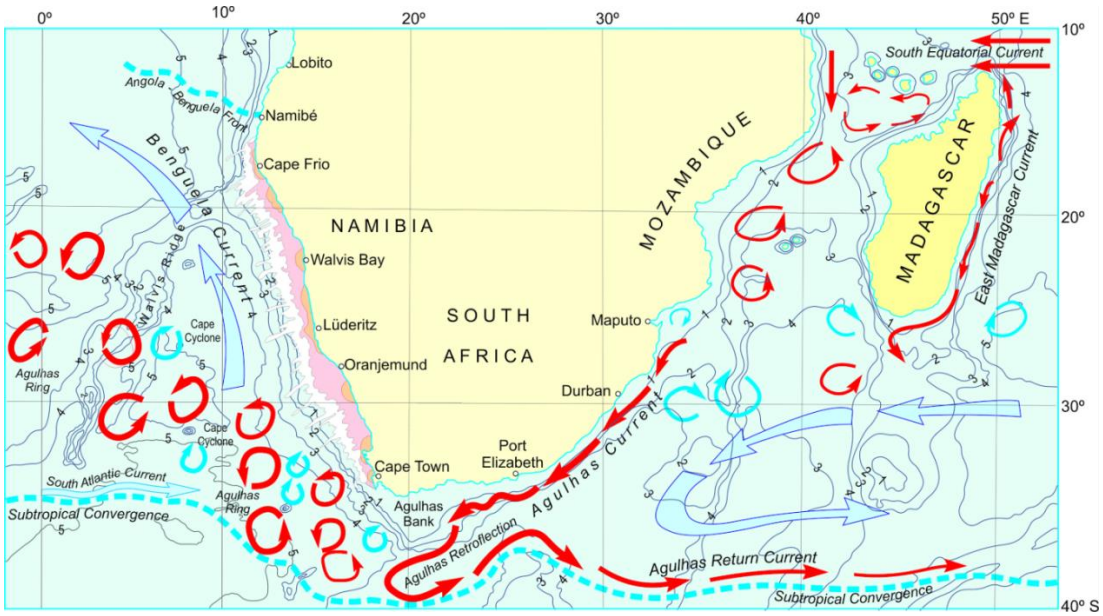

Figure 1 *Schematic of the entire Agulhas System, illustrating all the major features (Ansorge and Lutjeharms, 2007).*

1.1.1. Sources

The Agulhas Current has three major sources; water from the Mozambique Current, the Eastern Madagascar Current and the South-west Indian Ocean Sub-gyre (Lutjeharms and Webb, 1995). It has been found that the Agulhas is fed by a string of southward drifting, anticyclonic eddies coming from the Mozambique Channel (de Ruijter et al., 2002). The transport of water from the southern limb of the East Madagascar Current (EMC) has also been found to be in the form of both cyclonic and anticyclonic eddies, forming at the retroflection of the EMC (Quartly et al., 2006). The largest contributor of water into the Agulhas Current is the re-circulation of water in the South-west Indian Ocean Sub-gyre. Water peeling off the ARC is the major source of this re-circulated water (Gordon, 1985; Stramma and Lutjeharms, 1997).

Indian Ocean Tropical Surface Waters supplies the Agulhas current with lower salinity water (34.8-35.1) from the tropics (Gordon *et al*., 1987) while more saline (>35.4) South Indian Subtropical Surface Water is supplied by the South West Indian Ocean Gyre (Wyrtki, 1971).

1.1.2. Northern Agulhas Current

The Northern Agulhas Current, like the upstream sections of the Gulf Stream and Kuroshio, has an invariant path; the current closely follows the continental shelf. The stability of the current has been studied and the steepness of the continental slope has been cited as the reason for this (de Ruijter et al., 1999). The only place where this stability does not hold is at the Natal Bight; a wider part of the continental shelf in a coastal off-set north of Durban (Lutjeharms, 2007). The currents differing

behaviour is evident here; shear edge features, absent along the rest of the current, form here (Lutjeharms, 2007). The wider shelf at the Bight allows shear edge eddies to develop greater lateral expressions (Lutjeharms, 2007).

1.1.2.1. Natal Pulses

The stability of the Agulhas Current between Cape St. Lucia and the Agulhas Bank is interrupted at irregular intervals (De Ruijter *et al*., 1999), by the occurrence of solitary mesoscale meanders; dubbed "Natal Pulses" by Lutjeharms and Roberts (1988). These instabilities were first observed by Harris et al., (1978).

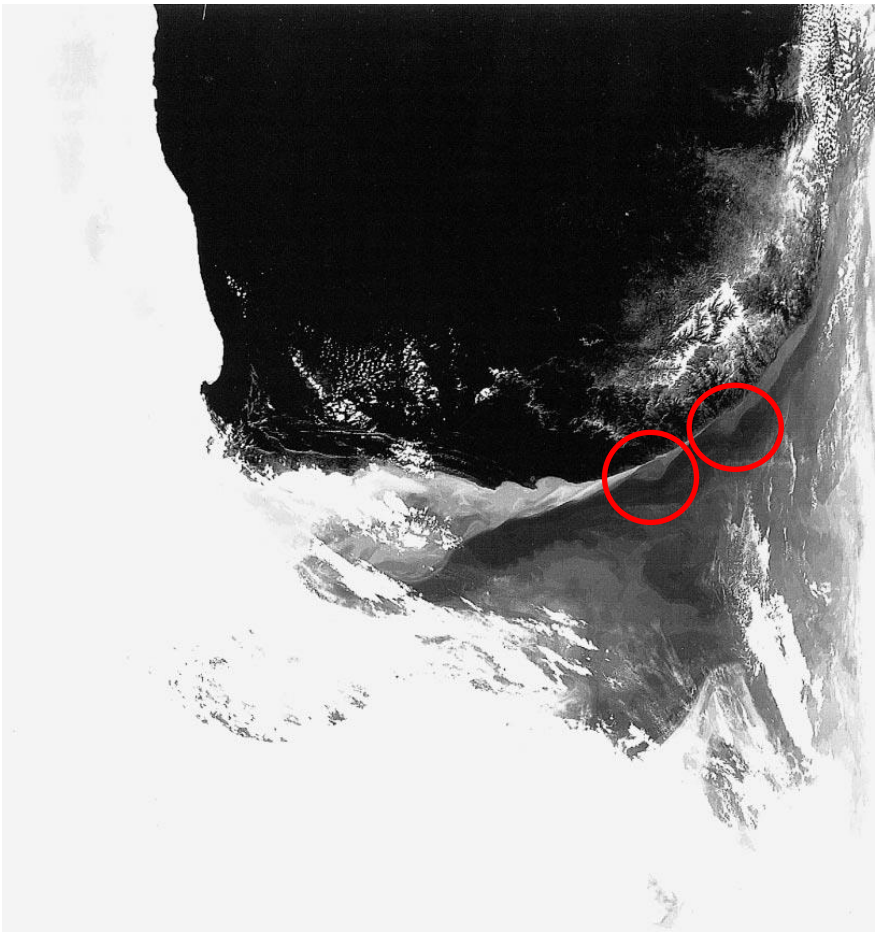

Figure 2 *NOAA infrared image. Grayscale from white (cold) to black (warm), with white clouds overhead. Two Natal pulses are visible as cyclonic meanders in the relatively dark (warm) Agulhas Current between Durban and Port Elizabeth (De Ruijter et al., 1999).*

Natal Pulses originate in the region north of Durban around a distinctive offset in the coastline, known as the Natal Bight, as the result of barotropic instability. These solitary cold water core meanders, with cyclonic circulation inshore of the Agulhas Current, move downstream at a rate of 10 to 20km/day (van der Vaart and de Ruijter, 2001; Lutjeharms, 2006; Grundlingh, 1979). Efforts to identify such meanders upstream of this offset have proved to be quite unsuccessful (De Ruijter et al., 1999).

Studies have found that an average of between 1 and 2 meanders progress into the Southern Agulhas region per year (Goschem and Schumann, 1990; Rouault and Penven, 2011). Observations from lagrangian floats have revealed that these meanders can extend to the full depth of the current (Lutjeharms et al., 2001), while other *in situ* studies have shown that these meanders can drive upwelling near the continental shelf (Bryden et al., 2005). Studies by Rouault and Penven (2011) showed that as these meanders move south, they grow and interact with topography to generate a secondary meander; either splitting, remerging or detaching from the primary meander. They also observed the generation of smaller eddies during the passage of one of these meanders; a possible indication of a decrease in energies towards the smaller scale, as well as a possible explanation for the decrease in the number of meanders observed as one moves further south.

1.1.3. Southern Agulhas Current

The continental shelf widens south of Port Elizabeth, to form the broad expanse of the Agulhas Bank. The current starts to develop meanders along the eastern edge of the shelf (Harris et al., 1978). These meanders have been seen to grow as they move down stream (Lutjeharms et al., 1989), and are accompanied by cyclonic eddies and warm plumes of water. At the northerly most point of the Agulhas Bank, close to Port Elizabeth, persistent upwelling was noticed (Lutjeharms, 2007). Once the current passes the southern tip of the Agulhas Bank, it proceeds into the South Atlantic as a free inertial jet (Lutjeharms et al., 1996). These filaments moving into the South Atlantic have been observed to carry anomalous amounts of warm and salty water into Atlantic, however their contributions to inter-ocean heat exchange is minimal, due to a loss of heat to the atmosphere (Walker and Mey, 1988), however their mass transport cannot be ignored (Lutjeharms, 2007).

1.1.4. Agulhas Current Transport

The Agulhas, like the North American Gulf Stream, is a fast-moving current with a large water transport. Geostrophic estimates of Sverdrup transport for the Agulhas, made for the 100 km inshore span adjacent to Durban, on the South African east coast, show a transport of 44 Sv (Toole and Raymer, 1985). Direct observations made by Grundlingh (1980) show a transport of 62 Sv for the upper 1000m. When extrapolated down to the sea floor, this transport figure increases to 75 Sv (Grundlingh, 1980). Beal et al., (2011) have measured the mean transport of the Agulhas at 32^{o}S to be 70 Sv, also noting a high interannual variability of the current of around 9 Sv. The wind stress curl across the Indian Ocean at 30^{o}S yields an additional transport of 30Sv based on Sverdrup dynamics (Hellerman and Rosenstein, 1983).

1.1.5. The Agulhas Retroflection

The Agulhas Retroflection occurs south of the Agulhas Bank, 39^{o}S, and between 16^{o} and 20^{o}E, with a loop diameter of 340km (Dencausse et al., 2010). This is the region where the westward-flowing Agulhas Current loops back onto itself and begins to flow eastward. This retroflection forms the western closure of the South Indian Ocean subtropical gyre. The reason that the Agulhas retroflects is not clear. There are a few mechanisms considered for the formation of the Retroflection inertia, the beta-effect and side-wall friction, all are thought to play a role, but in unknown proportions (de Ruijter, 1982).

The Retroflection plays an important role in water exchange between the Indian and Atlantic Oceans (Dencausse et al., 2010), through the shedding of large Agulhas Rings as well as through filament leakage of Agulhas water. Beal et al., (2011) have estimated the transport from this leakage to be between 2-15 Sv per year, estimating between 4-6 ring shedding events occurring within the same period. In recent studies, it has been suggested that due to anthropogenic climate change, transport through Agulhas leakage is increasing (Beal et al., 2011).

Gordon et al., (1987), using shipboard investigations, highlighted the key role that the Retroflection plays in the ventilation of the Atlantic and Indian Ocean thermocline, through the water transfer south of Africa (Gordon, 1985). Lutjeharms and Ballegooyen (1988) found the Retroflection to have a pulse-like behaviour. A study using satellite imagery showed the instability of the Agulhas Retroflection and how it could coalesce to form Agulhas Rings (Lutjeharms, 1981b) with an average diameter of 320km (Lutjeharms, 1981a).

The westward extent of the retroflection was shown by Lutjeharms and Ballegooyen (1984) to have little to no correlation with the intensity of the Agulhas current, and no defined seasonality was observed. However, a more recent study by Matano et al., (1998), using satellite altimetry, showed the retroflection to occur further east during the summer, and protrude further west during the winter. The influences of local winds were thought to be responsible for an increase in inertial re-circulation and force an early retroflection during the summer, as opposed to in winter (Matano et al., 1998). Detecting seasonal variability in the retroflection region has proved to be problematic, possibly due to the presence of superimposed inter-annual components in the region (Lutjeharms and van Ballegooyen, 1988)

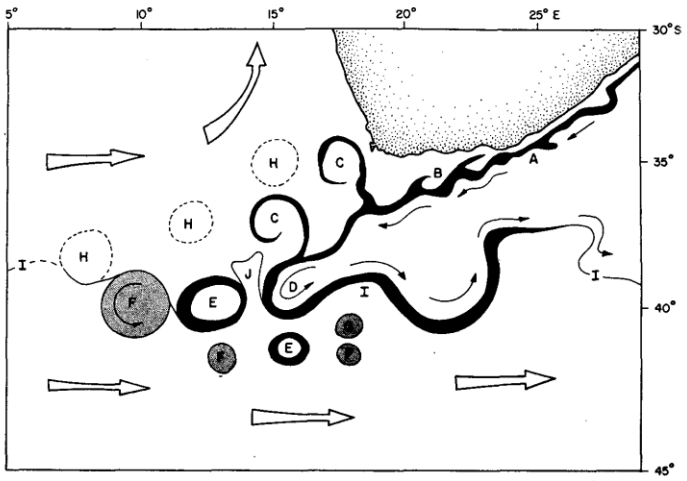

Figure 3 *A conceptual image, based on 7 years of satellite imagery and XBT section, of the Agulhas Retroflection and environment. Broad open arrows show mean drift patterns, while solid arrows show the current direction in the southern reaches of the Agulhas Current. Lettered features are: A, the narrow, well-defined surface expression of the Agulhas Current adjacent the narrow continental shelf of south eastern Africa; B, meanders in the current path next to the Agulhas Bank; C, Agulhas rings delineated by warm Agulhas filaments; D, the Agulhas Retroflection loop; E, newly spawned Agulhas rings, of which surface features are identifiably rings; F, older Agulhas rings which can no longer be unambiguously identified as rings by their surface expressions alone; G, a warm eddy south of the subtropical convergence, having been shed in the vicinity of the subtropical convergence; H, older Agulhas rings no longer evident by surface expressions; I, the subtropical convergence; J, wedge of cold Sub-Antarctic water (Lutjeharms and van Ballegooyen, 1988).*

1.1.6. The Agulhas Return Current

The Agulhas Return Current (ARC) emerges from the Agulhas Retroflection (Bang, 1970), flowing eastward. The structure of the ARC resembles that of the Agulhas Current, with a width of 60-80km and a transport of +-44 Sv, above 1000m (Boebel et al., 2002). Peak eastward surface velocities of the ARC reach up to 2 $m.s^{-1}$ near the retroflection, and decrease to around 1 $m.s^{-1}$ around 32°E (Boebel et al., 2002).

The trajectory of the ARC has high levels of variability (Lutjeharms and Ansorge 2001). Drifting buoys (Grundlingh, 1978; Daniault and Menard, 1985; Hoffman, 1988) showed that the general motion of the ARC is zonal, with meridional excursions which are possibly influenced by changes in bottom topography (Darbyshire, 1972; Lutjeharms and van Ballegooyen, 1984). The general location of the ARC starts at 39°30'S and moves further south to 44°30'S as it flows eastward (Lutjeharms and Ansorge, 2001). The ARC undergoes an equatorward meander over the Agulhas Plateau as it progresses east, illustrating the influence of bottom topography on its flow trajectory stated by Darbyshire (1972), and Lutjeharms and van Ballegooyen (1984). This equatorward meander over the Agulhas Plateau is what causes the ARC to come into close proximity of the Agulhas Current; the

magnitude of the meander determines the distance between the two currents. A large meander could cause and Agulhas Narrowing event or, if large enough, an early retroflection.

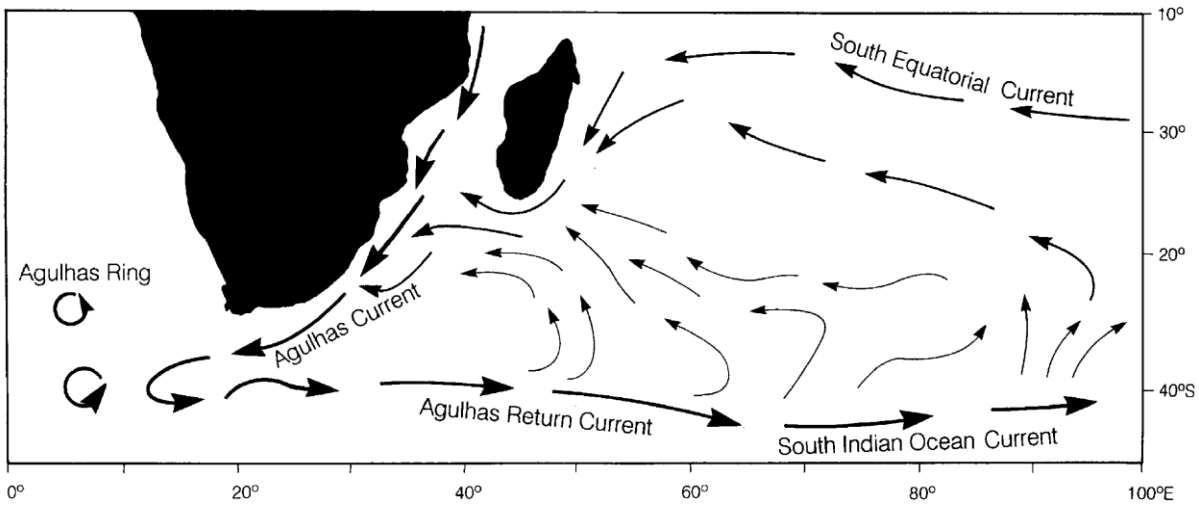

Figure 4 *A conceptual portrayal of the Agulhas Return Current as a component of the greater Agulhas Current System (modified from Lutjeharms and van Ballegooyen, 1988; Stramma and Lutjeharms, 1997).*

Water characteristics in the ARC, show a distinct modification from the Agulhas Current waters and all signs of the Indian Tropical Surface Water are removed at the retroflection (Lutjeharms and Ansorge, 2001). The ARC terminates at the Crozet Basin, where all traces of the Return Current have been removed (Lutjeharms and Ansorge, 2001).

1.1.7. Agulhas Rings

The advection of Agulhas Rings is one of the major components in the Indo-Atlantic exchange of water south of Africa (Lutjeharms, 1996; de Ruijter et al., 1999). These rings form south of the Agulhas Bank, the region at which the Agulhas Current loops back onto itself, retroflects (Lutjeharms and van Ballegooyen, 1988). The current loop created at the retroflection, occasionally occludes to form a distinctive ring of Agulhas water, which then advects into the South Atlantic (Lutjeharms and Gordon, 1987).

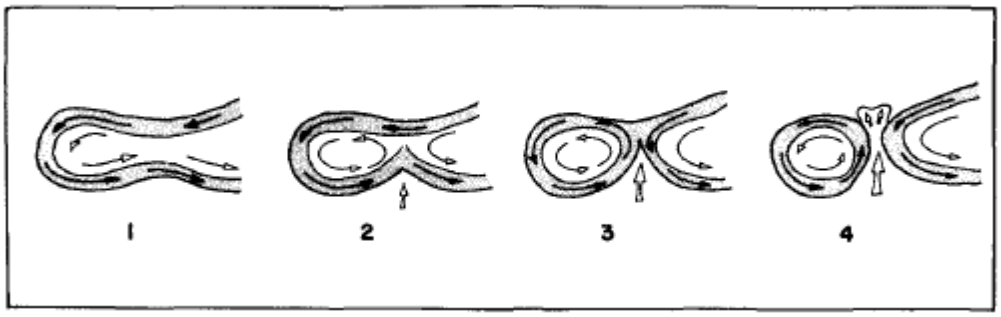

Figure 5 *Conceptual image of the initiation (2), development (3), and separation of an Agulhas ring from the Agulhas Retroflection (Lutjeharms and van Ballegooyen, 1988).*

These rings start off having all the physical and chemical characteristics of Southern Agulhas Current (Lutjeharms, 2007). Agulhas Rings have an average surface diameter of 240 +- 40 km, and azimuthal speeds between 0.29 and 0.9 m/s at the surface (Duncombe Rae, 1991). Lutjeharms et al., (2000) found that Agulhas Rings can extend the full depth of the ocean water column; findings by van Aken et al., (2003) showed that rings reached 4500 m, supporting Lutjeharms findings. Rings come in various shapes and sizes, behave differently from each another, and are differently affected by ambient waters and circulation (Lutjeharms, 2007). They move away from their point of origin at a rate of 5 to 8 km/day (Olson and Evans, 1986).

Once shed, these rings move into in an area known as the Eastern Cape Basin (Goni et al., 1997; Duncombe Rae 1991; Duncombe Rae et al., 1996). A number of rings and eddies may coexist here and interact with each other (Boebel et al., 2003a). Rings can split, merge or break into multiple parts; many never leaving the Cape Basin but dissipating there completely. Those that leave the Cape Basin must cross the Walvis Ridge on their passage into the South Atlantic (Lutjeharms, 2007). Byrne et al., (1995) established that Agulhas Rings do not travel north of 20^{o}S and rapidly lose kinetic energy after shedding; Schouten et al., (2002) determined that Rings lose up to 70% of their kinetic energy within their first 5 months.

Agulhas Rings are considered to be the largest contributor to the Indo-Atlantic inter-basin exchange of heat and salt (Gordon, 1985). Now with the intensity of Agulhas Leakage on the rise (Biastoch et al., 2009), speculation over its influence on the Atlantic Meridional Overturning Circulation (AMOC) has arisen. Beal et al., (2011) hypothesised that an increase in Agulhas Leakage could counteract the slowing AMOC, due to increased Arctic ice melt in a warming climate.

2. Data Assimilation System

The term 'data assimilation' originated in meteorology describing the use of observations to improve the forecasting skill of operational meteorological models (Rizzoli, 1996). Lewis Fry Richardson was the first scientist to attempt a numerical weather prediction in 1922. His attempt was a failure due to inappropriate smoothing of observations in his initial conditions, viewed as a deficiency with data assimilation (Blayo et al., 2011). Data assimilation and prediction systems have significantly improved since then, with new predication systems and assimilation techniques being developed. The purpose of data assimilation is to create a best estimate of a system state by using multiple sources of information (Blayo et al., 2011). In the oceanographic context, assimilation has three main objectives, firstly to improve the ocean model parameterizations of sub-grid scale processes, boundary conditions and unobserved sub-surface components. Secondly to produce a 4-dimensional representation of the oceanic flow that is consistent with both observations and a dynamical ocean model. Thirdly, to provide accurate initial conditions for ocean circulation modelling (Rizzoli, 1996); accuracy of a forecasts from numerical prediction models are dependent on the accuracy to which the initial state is known and the accuracy of the model (Daley, 1991).

Numerical models can be statistically accurate when compared with broad observational estimates, however when compared at specific times and locations, there are large discrepancies. Ocean models are an imperfect representation of the ocean system due to simplified mathematical parameterization of complex processes, as well as error from several factors. Even a perfect model can contain error, small errors in the initial state of the system will grow larger with time due to the non-linearities in underlying dynamics, a principle known as the Butterfly Effect (Lorenz, 1963). Therefore, synchronising the model state with the truth, existing and imperfect observations, is needed. Synchronisation must be repeated frequently to maintain a low error level in the system. Observations, from which we create initial conditions, also contain error. They are imperfect representations of the true ocean state due to measurement error and the usage of point measurements to describe broader ocean conditions (Edwards et al., 2015). Data assimilation attempts to bridge the gap between observations and numerical models and reduce the error of the resulting prediction system, by combining the two.

Ocean forecasting systems and data reanalyses producers are dependent on access to regularly available, near real time observational data, a well-developed numerical model, and a data assimilation scheme that has been proven to be effective in a region with similar dynamics (Backeberg et al., 2014). The first data assimilation experiment that focused on the Agulhas System using HYCOM, assimilated along-track SLA data (Backeberg et al., 2014). The primary rationale for assimilating

satellite altimetry data was that the mesoscale variability, and signals were accurately captured and well resolved, and thus the assimilation of SLA was expected to be able to constrain the model dynamics in a realistic manner (Backeberg et al., 2014).

The SLA assimilation proved to be an improvement over the free running, unassimilated model, in almost all respects. The weaknesses of the SLA assimilation over the free run are mainly due to SSH biases and incorrect correlations in the static ensemble (Backeberg et al., 2014), one of the areas where the assimilation of SST was expected to make an improvement. The static ensemble, or historical ensemble, based on a hind cast simulation from 1998-2007; it provides information about the mean circulation and variability of the region. The static ensemble aims to represent the forecast error of the model, and is used to calculate the background error covariance matrix. Biases in the static ensemble can create incorrect correlations in the assimilation, can cause errors in the EnOI when calculating the background covariance errors, creating incorrect positioning of currents, and thereby resulting in a poor representation of the flow in the assimilated models.

A regional implementation of HYCOM was used in this study, as HYCOM had been shown previously to be able to recreate the dynamics in the region with an accuracy deemed acceptable (Backeberg et al., 2008, 2009; Backeberg and Reason, 2010). This model was used in the previous study by Backeberg et al., (2014). The Ensemble Optimal Interpolation (EnOI) data assimilation scheme was used as it is 3-dimensional and multivariate, and updates the model at an efficient computational cost (Backeberg et al., 2014). This scheme has been previously utilised in regions with similar dynamics, like the Australian region (Oke et al., 2007), the Gulf of Mexico (Counillon and Bertino, 2009a; Srinivasan et al., 2011) and the South China Sea (Xie et al., 2011), which suggested it would be well-suited to the Agulhas region.

2.1. HYCOM

As a primitive equation model, HYCOM, uses a set of differential equations to approximate the ocean flow. HYCOM merges the best features of isopycnic-coordinate, and fixed-grid ocean circulation models within a single framework (Bleck, 2002). HYCOM identifies the optimal hybrid layer distribution for the model at each individual time step. It does this by interchanging between isopycnic (ρ) vertical coordinates when simulating the stratified open ocean, z-level coordinates while resolving upper-ocean mixed layer dynamic processes, and σ-coordinates in the shallow coastal regions (Backeberg et al., 2014). Priority is assigned to restoring the grid to isopycnic coordinates over the course of these vertical coordinate changes. Using this adaptive vertical grid enables the model to resolve regions of high vertical density gradients, such as the surface fronts and thermoclines (Backeberg et al., 2014).

A nested configuration containing two model domains is utilised; with a basin-scale HYCOM of the Indian and Southern Ocean (George et al., 2010) providing boundary conditions to a regional HYCOM of the Agulhas region (Backeberg et al., 2008, 2009), stretching from 10^{o} – 50^{o} S and from 0^{o} – 60^{o} E. Boundary conditions from the outer model are transferred to the inner model every 6 h. Boundary variables which change slowly over time, such as temperature, salinity, layer interface and baroclinic velocities, are relaxed towards the outer model over a 20 grid cell buffer zone (Backeberg et al., 2014). The relaxation time scale is 13 h at the outermost grid point, decreasing by a factor of 4 with distance from the boundary (Backeberg et al., 2014). The methodology from Browning and Kreiss (Browning and Kreiss, 1982, 1986) is used for faster changing variables, like barotropic velocities and pressure.

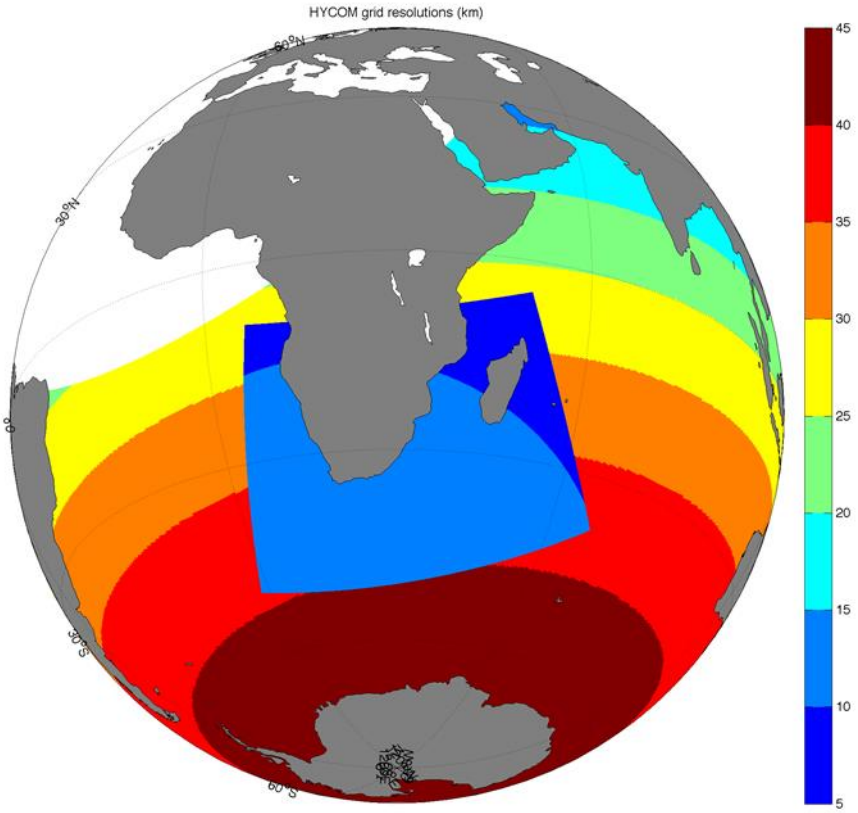

Figure 6 *Map of the model grid, illustrating the resolutions of the model in different regions.*

A conformal mapping tool (Bentsen et al., 1999) was used to create both the basin-scale and the nested model grid. The horizontal resolution of the basin-scale HYCOM varies from 45 km in the Southern Ocean, to 14 km in the northern Indian Ocean, and the resolution of the inner model is fixed at $1/10^{o}$ (Backeberg et al, 2014). The Rossby radius of deformation across the entire domain is around 30 km (Chelton et al., 1998); with the nested model known to be able to resolve eddies, shown in the previous study (Backeberg et al., 2014). Both inner and outer models contain 30 hybrid layers, with 3 m set as the minimum layer thickness in the upper layers (Backeberg et al., 2014). The reference

densities to which these hybrid layers refer to range from 23.6 to 27.6 kg/m3. To capture the salinity maximum within the Mozambique Channel, between 150–300 m, the interval between layer densities was increased between 23.6 and 26.8 kg/m^3 (Table 1). Similarly, to improve the resolution across the salinity minimum in the South Atlantic, between 600 and 1,200 m, the layer interval was reduced to between 27.1 and 27.7 kg/m^3 (Backeberg et al., 2014).

Table 1 *Summary of selected model parameters and numerical choices (Backeberg et al., 2014).*

Bathymetry	***GEBCO 1' resolution interpolated to model grid.***
Target densities (+1,000 kg/m3) *(layer 1 - layer 30)*	22.30, 22.60, 22.90, 23.20, 23.50, 23.80, 24.10, 24.40, 24.70, 25.00, 25.30, 25.60, 25.90, 26.20, 26.50, 26.80, 26.89, 26.99, 27.08, 27.18, 27.27, 27.37, 27.46, 27.56, 27.65, 27.75, 27.84, 27.94, 28.00, 28.05
Deformation-dependent biharmonic viscosity factor	0.20
Diffusion velocity (m/s) for Laplacian momentum dissipation	0.005
Diffusion velocity (m/s) for biharmonic momentum dissipation	0.06
Diffusion velocity (m/s) for biharmonic thickness diffusion	0.005
Diffusion velocity (m/s) for Laplacian temperature / salinity diffusion	0.005
Momentum advection scheme	second order
Vertical mixing scheme	KPP

Levitus climatology (Locarnini et al., 2006; Antonov et al., 2006) is used to initialise the outer model. The climatology is based on WOA05, which at the time of implementation of the model was the latest available version, but has since become outdated and will be updated in the next iteration. The outer model is spun up for 10 years, using climatological forcing from ERA-interim (Dee et al., 2011). A balanced field from the outer model is then used to initialise the inner model, interpolated to the high-resolution grid (Backeberg et al., 2014). Both models were run using the inter-annual atmospheric forcing fields from ERA-interim reanalysis data, over the period 1980 - 2007, with the outer model providing boundary conditions to the inner model (Backeberg et al., 2014).

Momentum fluxes are calculated following the approach by Kara et al., (2000), while the heat fluxes are calculated using the Drange and Simonsen method (1996). Monthly river outputs from the hydrological model: TOTAL Runoff Integrating Pathways (TRIP, (Oki and Sud, 1998)) are used. The data incorporates all river run-off input in the domain covering a period of 20 years, from ERA-interim. River

inflow is considered as a negative salinity flux, freshwater inputs, possessing an additional mass exchange component (Schiller and Kourafalou, 2010). The salinity flux is applied to a 6-m thick layer. To prevent large instabilities from being created near river deltas, the river flux is distributed over half an ellipsoid area, with the flux weight decreasing exponentially with distance from the source (60 × 200 km). Salinity relaxation is a method used to deal with inaccuracies in precipitation, evaporation and runoff (Backeberg et al., 2014). Backeberg et al., (2014) employed this surface relaxation of salinity method on monthly climatologies from the Polar science centre Hydrographic Climatology (Steele et al., 2001), which combined data from the World Ocean Atlas with the Arctic Ocean Atlas, in order to constrain them. The same approach was utilised in this study.

The HYCOM source code version 2.2 was used for both this and the previous study, as it included several improvements over the previous version 2.1 (Wallcraft et al., 2009). HYCOM 2.1 applied a simple vertical interpolation scheme to the mixed layer, which resulted in enhanced, and artificial, diapycnal mixing in the mixed layer, causing diffused surface velocity (Backeberg et al., 2014). Using version 2.1, Backeberg et al., (2009) showed that a fourth-order momentum advection scheme significantly improved the representation of the Agulhas Current core, although the observed current velocities were still stronger than those able to be simulated by the model (Backeberg et al., 2010). Unfortunately, the forth-order advection scheme in HYCOM version 2.2 is not yet fully functional, however Backeberg et al., (2014) found that the second-order advection scheme was able to provide a reasonably accurate reproduction of the mean circulation, with reasonable levels of mesoscale variability; particularly in the Agulhas retroflection region.

Backeberg et al., (2014) showed that the free running model had a mean SSH bias associated with an incorrect positioning of the Agulhas Return Current region. They suggested that this was likely caused by biases present in the boundary forcing of the outer model, where the Antarctic Circumpolar Current and the inflow from the eastern boundary of the domain is too weak, partly explaining the bias noted in the regional model (Backeberg et al., 2014).

2.1.1. Browning and Kriess approach to lateral boundary conditions

Shallow water equations have two times scales and are a symmetric hyperbolic system. Slow time scale motions are known as Rossby waves, while fast time scale motions are known as inertial/gravity waves. Browning and Kriess (1982) proved the existence of smooth solutions, solutions with multiple space and time derivatives on the order of Rossby wave time scales, for the open boundary problem of shallow water equations by using the bounded derivative method. The method required several initial time derivatives of the order of the slow time scale, and also boundary data that was smoothed.

They showed that if the boundary data was smooth, and only had small errors, then the solution of the open boundary problem would also be smooth, and only contain small errors produced in the interior. Alternatively, when boundary conditions were smooth, but contained large errors, then the open boundary solution remained smooth. However, the boundary error would propagate into the interior at speeds associated with the fast time scale, resulting in the destruction of the solution within a short time. It is therefore necessary to keep the boundary error small, to accurately compute the solution (Browning and Kriess, 1982). They also showed that the restrictions can be relaxed, allowing for only the large-scale boundary data to be correct. This approach was adopted in the HYCOM model.

2.1.2. Efficient and accurate bulk parameterizations of air-sea fluxes for use in general circulation models

Bulk formulae were used to calculate the momentum and heat fluxes in the numerical model. These formulae are computationally efficient and inexpensive and were developed for Global Circulation Models (GCM). They can calculate the effects of dynamic stability, wind stress and the heat fluxes at the air-sea interface.

These formulae contain a simple polynomial dependence on wind speed, and a linear dependence on the air-sea temperature difference, calculated from the statistical analysis of global monthly climatologies based off air-sea temperature and wind speed intervals (Kara et al., 2000). Kara et al., (2000) showed that by using surface observations from a mooring in the Central Arabian Sea and these formulae, it was possible to reproduce daily air-sea fluxes. These fluxes were proven to be definitively more accurate when compared to the fluxes calculated with a standard algorithm used by the Tropical Ocean Global Atmosphere Coupled Ocean–Atmosphere Response Experiment (TOGA COARE).

These formulae were used in this study as well as the previous by Backeberg et al., (2014). The formulae and parameterizations were shown to be less computationally expensive, while being more efficient, and substantially faster than the TOGA COARE bulk formula, since iterative calculations of wind stress and heat fluxes are not required (Kara et al. 2000), making them perfect for high resolution models such as the one utilised in this study.

2.2. Ensemble Optimal Interpolation

The Ensemble Optimal Interpolation scheme (EnOI) is a data assimilation scheme derived from the Ensemble Kaman Filter (EnKF). The EnOI (Evensen, 2003; Oke et al., 2002) scheme performs with greater computational efficiency than the EnKF method. It uses the static ensemble ($A \in \mathbb{R}^{n \times N}$, with N the ensemble size and n the model state dimension) to approximate the system background error covariances (**C**). The EnOI assumes that climatological variability is representative of the forecast error developed within an assimilation cycle (***ϵ***; Oke et al., 2002; Evensen, 2003).

$$\overline{\boldsymbol{\epsilon}\boldsymbol{\epsilon}^T} \approx C = \frac{\alpha}{N-1} A'(A')^T,$$

where $\boldsymbol{A' = A - \bar{A}}$ is the ensemble anomaly, and α is constantly used to adjust the variance of the ensemble. The method enables dimensional and multivariate changes that are consistent with the linear component of model physics (Counillon and Bertino., 2009a).

The static ensemble is derived from the Agulhas HYCOM and is sampled every five days over the period from 1998–2007. The model has been spun-up prior to the sampling period to avoid model drift, which can produce artificial erroneous correlations (Backeberg et al., 2014). The static ensemble is important to the EnOI because it represents the forecast error of the model, utilising the concept of ergodicity. Ergodicity or ergodic theory is a statistical mechanism whereby a sample size or sequence of a process is statistically representative of an entire process. The reasoning being that a collection of random samples from a process must represent the average statistical properties of the entire process, if the process changes erratically and at an inconsistent rate then it is not ergodic.

In the Agulhas region, the major source of error that develops during a single assimilation cycle was expected to be caused by the incorrect placement of mesoscale features, such as eddies and meanders (Backeberg et al., 2014), with these features interacting with both the residual current and the underlying bathymetry.

When assimilating SLA in Backeberg et al., (2014), it was expected that concurrent hydrographic changes would occur due to correlations between SSH and the water masses of the mesoscale features. An example of this was a scatterplot between SSH and SST, from the static ensemble in the Agulhas Current at 30°E and 32°S (see Fig.3 in Backeberg et al., 2014). It was shown that no correlation between SSH and SST was present when the correlation was calculated for the 10 year static ensemble (Backeberg et al., 2014).

After calculating the correlation across the different seasons, it became noticeable that the correlation was seasonally enhanced, particularly over the winter period (Backeberg et al., 2014), June–July–August (R = 0.4). The static ensemble had to be adjusted to limit the season variability impact on the correlation matrix of the EnOI.

The static ensemble utilised by Backeberg et al., (2014), and again in this study, to calculate the forecast error covariance is composed of a 60-day running window of ensemble states, which are then centred around the associated seasonal period, with respect to the assimilation time (Xie et al., 2011). The resulting ensemble contains 120 members, a relatively big sample size, which would reduce the noise in the spatial correlation (Backeberg et al., 2014).

The ensemble size is not large enough to cover the model variability over the entire domain, therefore any associated sampling errors would lead to the introduction of erroneous long-range spatial correlations (Backeberg et al., 2014). It would be illogical for an observation assimilated within the Retroflection region to contribute towards the resolution of an eddy in the Mozambique Channel (Backeberg et al., 2014). So, to limit the assimilated point's impact on other regions of the model, its influence is contained by confining it to a definitive local area, using Evensen's (2003) local framework method. By analysing the spatial correlations of SSH at different locations within the Agulhas system, Backeberg et al., (2014) concluded that 400 km is an appropriate localisation radius. To avoid discontinuities during the update, the innovation vector (i.e. the distance between the forecast and the observations) is tapered with respect to the distance from the observation using a Gaspari and Cohn function (Gaspari and Cohn, 1999), resulting in an effective localization radius of $\sim$100 km (Backeberg et al., 2014).

The entire model state of the forecast is updated through the multivariate properties of the EnOI, i.e. temperature, salinity, layer thickness, barotropic and baroclinic velocity, throughout the water column (Backeberg et al., 2014). This allows for the conservation of linear properties (Evensen, 2003) such as geostrophy, and ensures that the sum of the layer thickness matches the barotropic pressure (Backeberg et al., 2014). Srinivasan et al., (2011) showed that this approach performs well within the hybrid vertical framework of HYCOM.

The assimilation process follows the same order as in Xie et al. (2011). SSH is diagnosed from the model state, and SLA is calculated by removing the model mean (Backeberg et al., 2014). Anomaly assimilation ensures that the innovations over many assimilation cycles converge to 0, however this does not account for possible biases in the numerical model variability error (Backeberg et al., 2014).

Observations are generally sparse and sporadic across a temporal scale; it would therefore be impractical to stop the model at random intervals whenever an observation became available. To work around this, observations are collected and assimilated, as a batch, once a week. To constrain the model with such a limited number of observations, the multivariate covariance between one observation and the model grid needs to be calculated. At each point the model is projected into the observational space, a covariance matrix between the model and the observation is then constructed and weighted against the total error covariance, which is the sum of the model error covariance and the observation error covariance. This is then multiplied by the innovation factor, defined as the difference between the model and the observation. In determining the innovation factor, a first-guess approach is employed, where the model forecast (ψ^{f}), and the assimilated data (**d**) are then compared

for the same day (*t*0-i, where i corresponds to the day in the weekly forecast cycle). The new analysis state (ψ^{a}_{t0}) is then estimated as follows:

$$\psi^{a}_{t0} = \psi^{f}_{t0} + \sum_{i=0..6} A'_{t0} A'^{T}_{t0} \; H^T \left(H A'_{t0} A'^{T}_{t0} H^T + \frac{N-1}{\alpha} R \right)^{-1}$$

$$\left(\mathbf{d}_{t0-i} - H\psi^{f}_{t0-i} \right),$$

Where ***H*** is the measurement operator relating the prognostic model state variables to the measurements, and ***R*** is the observation error covariance matrix. For simplicity and computational efficiency, ***R*** is considered as a diagonal matrix, and its variance is determined as proposed by Oke et al., (2008):

$$\varepsilon_o^2 = \varepsilon_{instr}^2 + \varepsilon_{re}^2.$$

The observation error variance (ε_o^2) is the sum of instrument error (ε_{instr}^2) and the representivity error (ε_{re}^2). The latter is approximated by the sea surface height variance derived from satellite altimetry observations and has a similar impact to tuning the coefficient α, which was set to 1 to simplify the tuning process. By using satellite altimetry derived sea surface height variance, rather than dynamical model derived variance, the results of the assimilation experiment were improved (Backeberg et al., 2014).

3. Observations

In this study sea surface temperatures (SST) from OSTIA, together with along-track sea level anomaly (SLA) data from satellite altimeters, were assimilated into the model. Surface drifter data from the Global Drifter Program (GDP), persistence forecasts using altimetry data from AVISO data, and Argo profiling floats were used to validate the assimilation system.

3.1. Satellite Altimetry Data

All satellite altimetry data used in the study was produced by Ssalto/Duacs and distributed by AVISO, supported by CNES.

The delayed time unfiltered along-track SLA from satellite altimeters was assimilated into the model. This unfiltered data set was utilised because of the smoothing contained within the interpolation of the gridded product (Ducet et al., 2000), which can cause problems in a highly dynamic region such as the Agulhas. The unfiltered data can sufficiently sample the short spatial scales (Wunsch and Stammer, 1998), while the effects of aliasing are reduced (Byrne and McClean, 2008).

The unfiltered data has a 7-km resolution, with the temporal range of satellites in this study (2008-2009) including altimetry data from Jason-1 (until October 2008), Jason-2 (from October 2008), Jason-1 tandem mission orbit (from February 2009), ENVISAT and GFO (until September 2008; Backeberg et al., 2014).

To create a comparison between the assimilation system and persistence forecasts of SLA and geostrophic currents for the period 2008 - 2009, the delayed time along-track data set was used to reconstruct the gridded map data in a three-day delayed mode (Backeberg et al., 2014). A persistence forecast assumes that the conditions at present will persist into tomorrow, this method works well for short term forecasts as well as long term climatologies. The resulting maps were then combined with Rio09 mean dynamic topography (MDT; Rio et al., 2011) to calculate the surface geostrophic currents and eddy kinetic energies (EKE).

The main difference between the gridded data and delayed time maps from AVISO are in the temporal selection of measurements used to construct the map (Backeberg et al., 2014). The approach utilised to generate the data follows the method employed when processing data in the near real-time, with a three-day delay (Backeberg et al., 2014). However, this approach does not consider any problems regarding data availability, and data acquisition that could possibly occur during real-time processing. The delayed time along-track data is a higher quality data set than the near real-time data, mainly due to the level of orbit corrections and other data corrections employed during the processing stages.

The three day delayed maps are produced every 7 days and then persisted for a further seven day forecast cycle to allow for comparisons with the assimilation system (Backeberg et al., 2014).

3.2. Sea Surface Temperature Data

Once weekly satellite SSTs for that day, in addition to the along-track SLA data gathered over the week, are assimilated into the model. Despite SSTs being available daily, they are only assimilated once weekly to avoid stopping the model each day for assimilation. The SST data set used was obtained from the Operational Sea Surface Temperature and Sea Ice Analysis (OSTIA; available at http://ghrsst-pp.metoffice.com/pages/latest_analysis/ostia.html). OSTIA analysis uses satellite data from sensors that include the Advanced Very High Resolution Radiometer (AVHRR, (US National Oceanic and Atmospheric Administration)), Advanced Along-Track Scanning Radiometer (AATSR, (European Space Agency)), Spinning Enhanced Visible and Infrared Imager (SEVIRI, (European Organisation for the Exploitation of Meteorological Satellites)), Advanced Microwave Scanning Radiometer-EOS (AMSR-E, (NASA National Snow & Ice Data Centre)), and the Tropical Rainfall Measurement Mission (TMI, (US National Aeronautical and Space Agency)). The data set has a global coverage, with a grid resolution of 0.054 degrees, and a temporal resolution of one day. OSTIA is made available as the Group for High Resolution Sea Surface Temperature (GHRSST) product. The OSTIA analysis has a highly-smoothed SST field and was specifically produced to support SST data assimilation into Numerical Weather Prediction (NWP) models. One of the limitations of the smoothing process is that small, mesoscale features can be lost. In a highly dynamic region like the Agulhas mesoscale features play an important role, which might be removed by the smoothing thereby impacting the solution during assimilation. The OSTIA SST data was also used to validate the SSTs in system.

3.3. Drifter data

To determine the accuracy of the assimilation system against independent observations, surface velocity data from satellite-tracked surface drifting buoys or drifters are used. These drifters consist of a surface buoy and a 15 m deep subsurface drogue. The surface buoy measures temperature and records its position, which is then transmitted via a satellite. The data are managed and distributed by the Global Drifter Program (GDP, (NOAA AOML Physical Oceanography Division)), whose objective is to maintain a global 5x5^{o} array of ~ 1250 drifters. Due to sparse spatial coverage of drifter data in the region, all data from drifters that entered the region 5^{o} – 52^{o} S and 2^{o} – 69^{o} E between 1986 and 2012, a total of 1246 drifters, were used in the study. Only 115 drifters entered the region between 2008 and 2009. The raw drifter data is interpolated to 6 h positions, with surface *u* and *v* velocities and surface temperatures provided for each corresponding position (Backeberg et al., 2014).

3.4. Argo floats

To evaluate the impact of assimilating SST on the water masses within the model, Argo profiling floats are used. These data sets were collected and made freely available by the International Argo Program and the national programs that contribute to it (http://www.argo.ucsd.edu, http://argo.jcommops.org). The Argo Program is part of the Global Ocean Observing System. These Argo floats capture temperature and salinity profiles in the upper 2000m of the water column every $\pm$ 10 days, as well as their position when at the surface. Apart from temperature and salinity, the Argo floats also captured velocities at 1000 m, which form part of an Argo based deep displacement dataset known as ANDRO Atlas (Ollitrault and Rannou, 2013; available at http://www.coriolis.eu.org). During 2008-2009, 91 Argo floats entered the region between $12^{o} - 45^{o}$ S and $15^{o} - 45^{o}$E, and 2807 profiles of temperature and salinity were obtained. To validate the assimilated and unassimilated runs with the Argo data, the model outputs are interpolated to positions of these Argo profiles (Backeberg et al., 2014). In the study, only data where floats had a representative parking pressure (measured pressure averages, during a float's subsurface drift) between 900 - 1100 m, 399002 individual measurements during 2008 - 2009 were used (Backeberg et al., 2014).

4. Results

4.1. Surface and Subsurface Velocities

4.1.1. Surface Velocities

To allow for the comparison between AVISO, a free run (FREE), two assimilated runs ($ASSIM_{SLA}$ and $ASSIM_{COMBINED}$) and the *in situ* drifter data, the daily surface velocities from AVISO, FREE, $ASSIM_{SLA}$ and $ASSIM_{COMBINED}$ were interpolated to the daily latitudinal and longitudinal positions of the surface drifters, using the nearest neighbour method of interpolation. The drifters measure subsurface velocities at 15 m; this could induce a bias when compared to the model and satellite data, which record velocities at the surface, and must therefore be accounted for. It was assumed that there would be little difference between the surface and the 15 m subsurface velocities, due to the geostrophically dominated dynamics of the region. The 6-hourly *u* and *v* component velocities and their magnitudes derived from the surface drifters were averaged for each day and then and assigned to the median position along the drifter track for that day. Median positions of the drifters were used to ensure that the daily position and corresponding velocity was along the drifter's track. Using the daily mean position in some cases resulted in the longitude / latitude position to be offset from the drifter's trajectory, resulting in the daily mean velocity calculated for that day to be in a location offset from the drifter's trajectory. This may result in the daily average velocity not being representative of the dynamics along the drifter's trajectory.

After analysing the track of Drifter #71114 between 1 January 2008 and 1 July 2008, it was found that the velocity magnitudes of $ASSIM_{COMBINED}$ were more in line with that of the drifter derived velocities during the periods where the drifter was located around the edges of mesoscale eddies. The improvement is reflected in the correlations ($ASSIM_{COMBINED}$ = 0.45, $ASSIM_{SLA}$ = 0.39, FREE = 0.19, AVISO = 0.62), which give us an indication of the models ability to monitor the variability of the Agulhas System. However, the $ASSIM_{COMBINED}$ had a noticeable velocity bias between February 2008 and May 2008 and could also not perform as well as AVISO over the entire period. This bias can be explained by several factors, such as the comparison between subsurface and surface velocities. Fortunately, bias in a prediction system can be corrected in post-processing. Model and AVISO velocity magnitudes are generally over-estimated during this period; their mean velocities highlight this bias ($Mean_{Drfiter}$ = 0.49 m/s, $Mean_{AVISO}$ = 0.66 m/s, $Mean_{FREE}$ = 0.67 m/s, $Mean_{ASSIM\_SLA}$ = 0.69 m/s, $Mean_{ASSIM\_COMBINED}$ = 0.86 m/s). $ASSIM_{COMBINED}$ mean velocity is significantly higher than all the other estimates. The pre-existing velocity bias present in FREE and $ASSIM_{SLA}$ has been increased in $ASSIM_{COMBINED}$. A possible reason for this can be seen in Fig.7, where daily averaged surface velocity field snapshots, across the 3 model runs, illustrate the impacts of the SLA and SST assimilations. The high velocities seen in $ASSIM_{COMBINED}$

could have resulted from the small turbulent features introduced to the system by the assimilation of SST. This could be the result of the OSTIA SST data resolving smaller mesoscale features, not captured by the SLA products or simulated by the 1/10th of a degree model.

Another reason for the bias produced could be the result of comparing Lagrangian and Eulerian frameworks and how they measure different processes. Eulerian velocity is an averaged representation of velocities for a grid cell, while Lagrangian velocities, which are smaller, will measure more fine scale processes as the drifter will takes detours etc., resulting in a bias. Drifters also tend to gather in regions of weak dynamics which will create additional bias. This is a reason why getting a perfect correlation between drifter, model and AVISO velocities is very difficult, because they are in effect measuring different processes. Additionally, drifter measurements are impacted by ageostrophic components such as wind, this is not captured by AVISO and therefore leads to discrepancies. HYCOM does include an ageostrophic component, however the resolution is coarser than that of the drifters. These ageostrophic components are imperfect and contribute to the bias in the models. $ASSIM_{COMBINED}$ shows more sub-mesoscale features, which is more realistic than FREE and $ASSIM_{SLA}$, but it is penalized by the way the system is validated.

To quantify any improvement in the accuracy of this updated assimilation, the root mean squared error (RMSE) for the models and AVISO was calculated (Table 2), using drifter derived velocities from all available drifters entering the domain during 2008 and 2009. The analysis showed an increase of the RMSE in $ASSIM_{COMBINED}$ compared to $ASSIM_{SLA}$. The assimilation of SST has led to the introduction of other small scale turbulent features, mentioned earlier, which have impacted the accuracy of $ASSIM_{COMBINED}$ drifter tracking. From Fig.7, it is visible that FREE produces far too many eddies consistently propagating along the same trajectories. This was largely resolved by Backeberg et al., (2014) through SLA assimilation, which dampened the eddy energy offshore of the Agulhas Current. However, it appears that by assimilating SSTs, this improvement has been slightly degraded. The 5 km resolution SST data set introduced mesoscale features that the 10km resolution of the model is not necessarily able to resolve. Despite there no longer being this production line of eddies propagating along the offshore edge of the Agulhas Current, these smaller turbulent features could possibly account for the increase in the error of the velocity fields in $ASSIM_{COMBINED}$.

What is also interesting is how the assimilation of SST in $ASSIM_{COMBINED}$, affects the positioning of mesoscale features in comparison to $ASSIM_{SLA}$. Some features present in $ASSIM_{COMBINED}$ can be found in both FREE and $ASSIM_{SLA}$, while some features in $ASSIM_{COMBINED}$ are not present in either $ASSIM_{SLA}$ or FREE (Fig.7). This highlights the influence of the assimilation on the numerical model, as well as highlighting the SST assimilations impact on the resultant velocity fields. The biases, inaccurate

dynamics and weighting factors of the model and assimilated data must be re-evaluated in future iterations of the model to improve upon the error, and representation of the surface velocity fields. Although a slight improvement of accuracy over the FREE model run is evident in $ASSIM_{COMBINED}$, the assimilation is unable to provide a better forecast of surface drifter velocities than $ASSIM_{SLA}$ and AVISO, whose RMSE are still more accurate, ± 0.2 m/s for AVISO and ± 0.1 m/s for $ASSIM_{SLA}$.

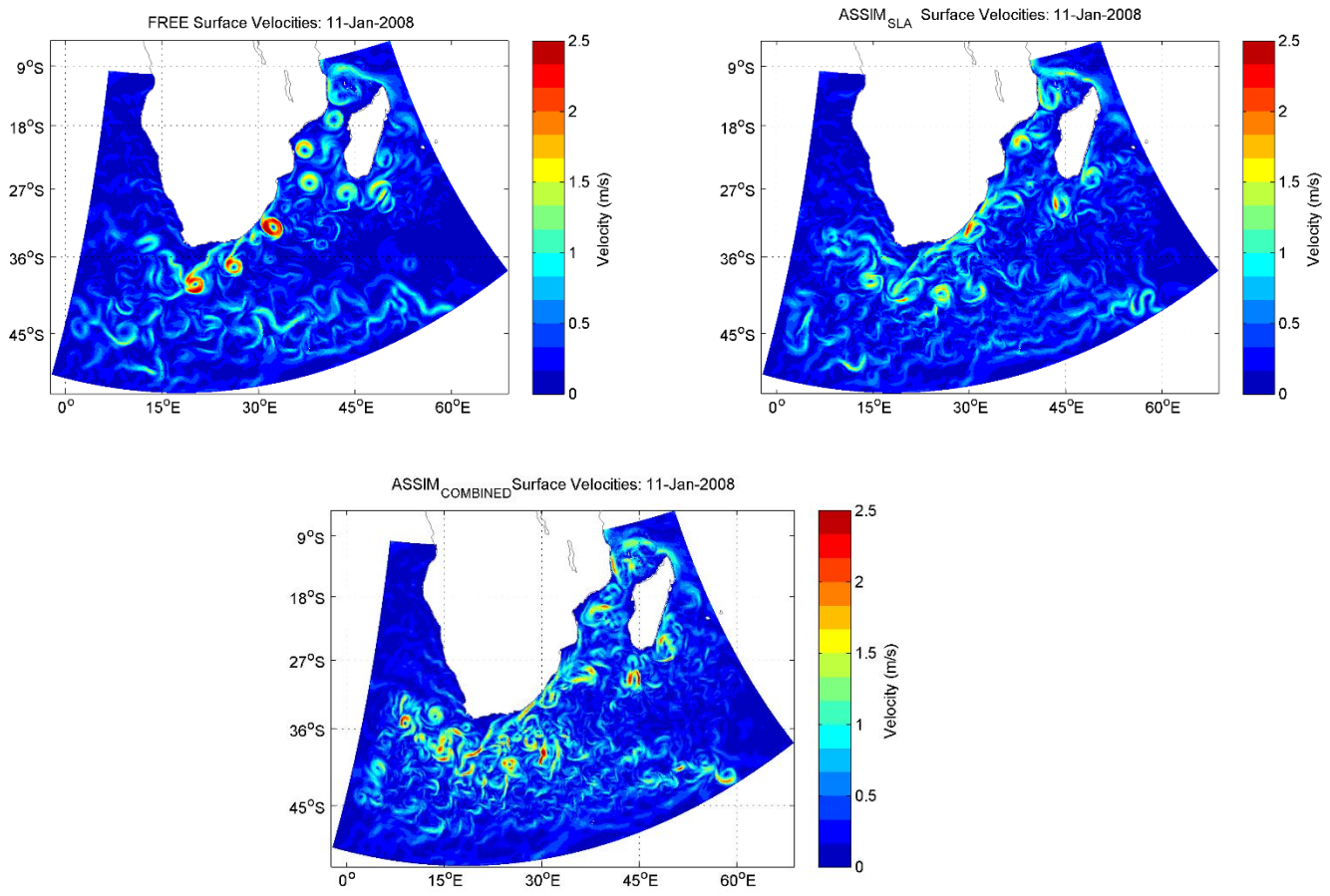

Figure 7 *Daily averages of surface velocities from 11 January 2008, highlighting the differences between the models.*

Table 2 *Correlation (R) of the u and v component velocities and RMSE of velocity magnitudes calculated against surface drifter observations from 2008 - 2009.*

	FREE	**$ASSIM_{SLA}$**	**$ASSIM_{COMBINED}$**	**AVISO**	**Drifters**
Bias	0.03	0.04	0.09	-0.05	-
$\mathbf{R}_{u \& v\ comp.}$	0.07	0.33	0.35	0.91	-
$\mathbf{RMSE}_{vel.\ mag.}$	0.31	0.26	0.30	0.18	-
$\mathbf{RMSE}_{bias\ free}$	0.094	0.070	0.092	0.032	-
$\mathbf{Mean}_{vel.\ mag.}$	0.306	0.314	0.363	0.203	0.263

The *u* and *v* component velocities can be used as a proxy to determine the accuracy of the model, when positioning and timing the placement of mesoscale features. Correlating vector quantities can be problematic, since vectors represent both magnitude and direction, and with direction also being a circular function (Backeberg et al., 2014). Therefore, a generalised vector correlation was used to calculate the *u* and *v* component correlations in both this and the previous study (Crosby et al., 1993).

The resulting *u* and *v* component velocity correlations, calculated using all available drifter data from 2008 - 2009, (Table 2) are better in $ASSIM_{COMBINED}$ compared to $ASSIM_{SLA}$ and FREE. Although when compared to AVISO ($R_{u \& v\ comp.} = 0.91$), $ASSIM_{COMBINED}$ ($R_{u \& v\ comp.} = 0.35$) is still significantly less correlated over same period. Again, we see the impact of resolving sub-mesoscale features through the assimilation of SST data into the model. The correlation of the velocity components has been improved in $ASSIM_{COMBINED}$ over $ASSIM_{SLA}$. Due to the models improved ability to resolve the smaller turbulent features, the placement and timing of these features has also been improved. Although the assimilation of SST has improved the correlation results of the model, it is still unable to match the results obtained from AVISO. In the previous study Backeberg et al., (2014) suggested that the strong correlation between AVISO and the drifter data, for *u* and *v* component velocities, was due to geostrophic balance dominating the circulation in the Agulhas Current system. This looks to still be the case as the resolution of these small-scale features, which do not necessarily follow the geostrophic balance, has only served to slightly improve the correlation of the model. The correlation of the AVISO fields is nearly three times that of $ASSIM_{COMBIONED}$, suggesting that the newly resolved filaments in $ASSIM_{COMBINED}$ do not significantly contribute to improving the mesoscale forecasts in the Agulhas System. It could also be that the observations used to validate the model were not able to capture the appropriate dynamics, creating a challenge to find appropriate observations with which to validate the assimilation system.

When we look at the RMSE, the error in the $ASSIM_{COMBINED}$ is found to be higher than that of the $ASSIM_{SLA}$ and AVISO, but still slightly better than FREE. This is again the case when considering the individual *u* and *v* components. The RMSE of the *u* component, is higher in $ASSIM_{COMBINED}$ than $ASSIM_{SLA}$ and AVISO, but still slightly better than FREE; the same holds true for the RMSE of the *v* component.

Examining the bias and bias free RMSE provides additional support for the previously discussed results. In the case of bias, FREE has the lowest bias of 0.029, $ASSIM_{SLA}$ follows with a 0.037 bias, AVISO has a negative of -0.053, lastly $ASSIM_{COMBINED}$ has the largest bias of 0.087 (Table 2). These biases are reflected in the mean velocity measurements, with FREE falling closest to the drifter mean, AVISO underestimating the mean, and $ASSIM_{COMBINED}$ significantly overestimating it (Table 2). The $RMSE_{bias\ free}$ corroborates the results found earlier, when RMSE was examined. AVISO has the least error overall, with bias removed, $ASSIM_{SLA}$ is the most accurate from the model runs, and $ASSIM_{COMBINED}$ is still fractionally more accurate than FREE (Table 2).

So, while the assimilation has improved the spatial representation of surface velocity fields, it has increased the bias in the model, and hindered its ability to capture the correct levels of velocity. This bias could be a result of the introduction of these small-scale filaments and processes which do not necessarily follow the geostrophic balance, as previously stated. The assimilation of features which the model cannot resolve on its own may introduce a level of variability into the system which is not necessarily physical, but associated with the difference in resolution between the model and the SST observation assimilated.

Fig.8 illustrates the difference between the mean velocity fields of $ASSIM_{SLA}$ and $ASSIM_{COMBINED}$. Many of the major differences are centred on the Southern Ocean, but there are also signs that show that $ASSIM_{COMBINED}$ has produced lower velocities along the Agulhas Current than $ASSIM_{SLA}$, on the order of nearly 0.2 m/s. These changes along the Agulhas Current, the region between 26^{o} – 36^{o} S and 22^{o} – 34^{o} E, were zoomed in on and analysed further.

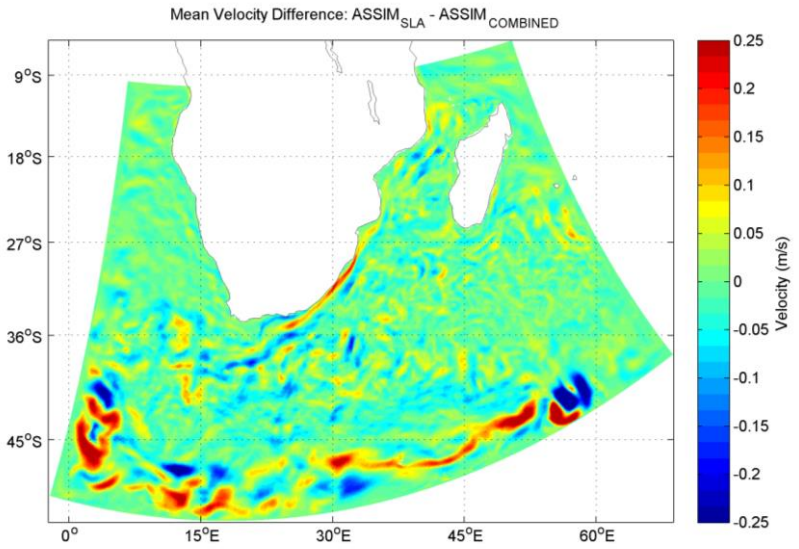

Figure 8 *Difference between the two-year mean velocity fields of ASSIM$_{SLA}$ and ASSIM$_{COMBINED}$.*

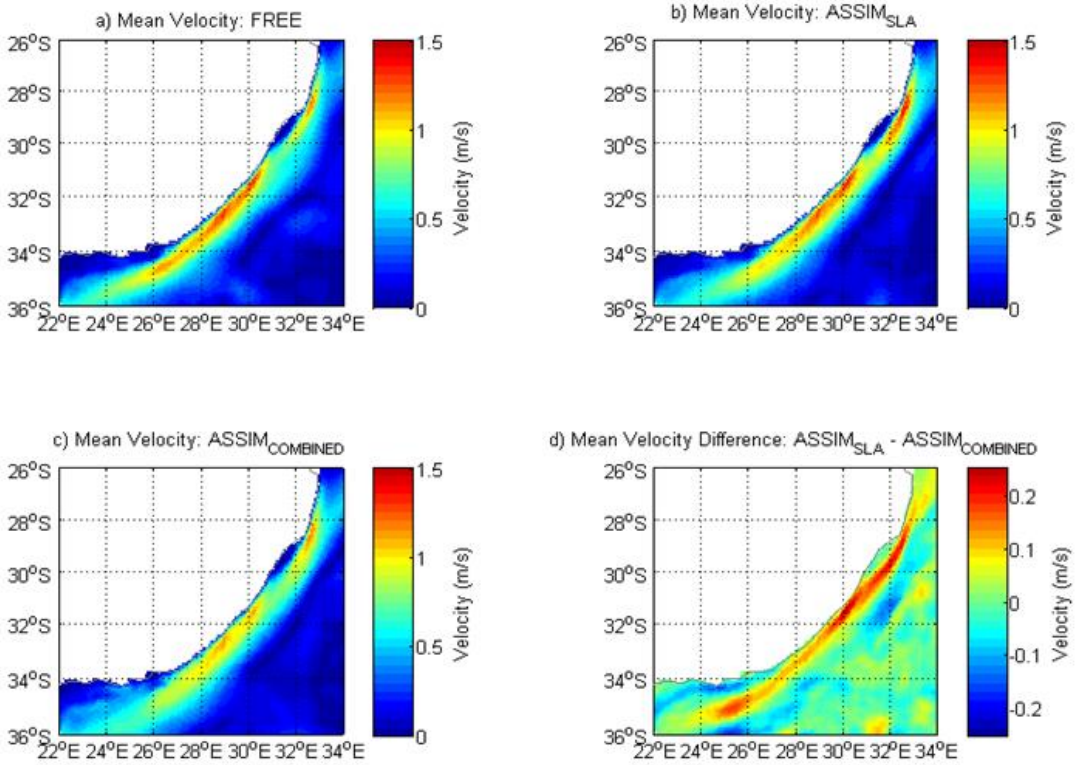

Figure 9 a) *2008 – 2009 mean velocity map from the FREE;* ***b)*** *mean velocity map from ASSIM$_{SLA}$;* ***c)*** *mean velocity map from ASSIM$_{COMBINED}$;* ***d)*** *Difference map, of mean velocities, ASSIM$_{SLA}$ minus ASSIM$_{COMBINED}$. Red colours indicate where ASSIM$_{SLA}$ has higher velocities than ASSIM$_{COMBINED}$, while blue indicates the opposite.*

From Fig.9 (a-c) the mean impact of assimilating different observations over the Agulhas Current is evident. FREE maintains high velocities along the Agulhas Current, extending further south, compared to both assimilations. This only differs north of the Natal Bight, where the velocities are reduced, like

that seen in $ASSIM_{COMBINED}$. FREE and $ASSIM_{SLA}$ show velocities up to 1.4 m/s along the Agulhas Current, while $ASSIM_{COMBINED}$ only contains velocities up to 1.2 m/s. FREE produces a narrower Agulhas Current as compared to $ASSIM_{SLA}$ and $ASSIM_{COMBINED}$, with $ASSIM_{COMBINED}$ simulating the widest current. Fig.9d illustrates the difference the additional assimilation of SST has had compared to $ASSIM_{SLA}$. The most notable difference is in the core of the Agulhas Current. Here the surface velocities in $ASSIM_{SLA}$ are up to 0.25 m/s higher than in $ASSIM_{COMBINED}$. There are also areas, adjacent to the current and inshore of the current south of Port Elizabeth, where $ASSIM_{SLA}$ is around 0.2 m/s lower than $ASSIM_{COMBINED}$.

To better quantify these differences a quantile-quantile (QQ) analysis was performed for the zoomed in region (Fig.10). This compares *in situ* drifter derived velocities against the corresponding simulated velocities. Simulated velocities that lie closer to the drifter magnitudes are more accurate than those further away. From Fig.10 it is visible that the FREE and $ASSIM_{SLA}$ are more accurate at producing surface velocities when they are below 1 m/s, with FREE being the most accurate. While $ASSIM_{COMBINED}$ is shown to be more accurate when velocities are above 1 m/s, $ASSIM_{COMBINED}$ over-estimates velocities below 1 m/s, while $ASSIM_{SLA}$ over-estimates velocities over 1 m/s (Fig.10). AVISO on the other hand consistently underestimates the velocities, consistent with the bias presented earlier. It must be noted that the optimal interpolation method, used to construct these maps and plots, tends to overestimate low velocities and underestimate high velocities.

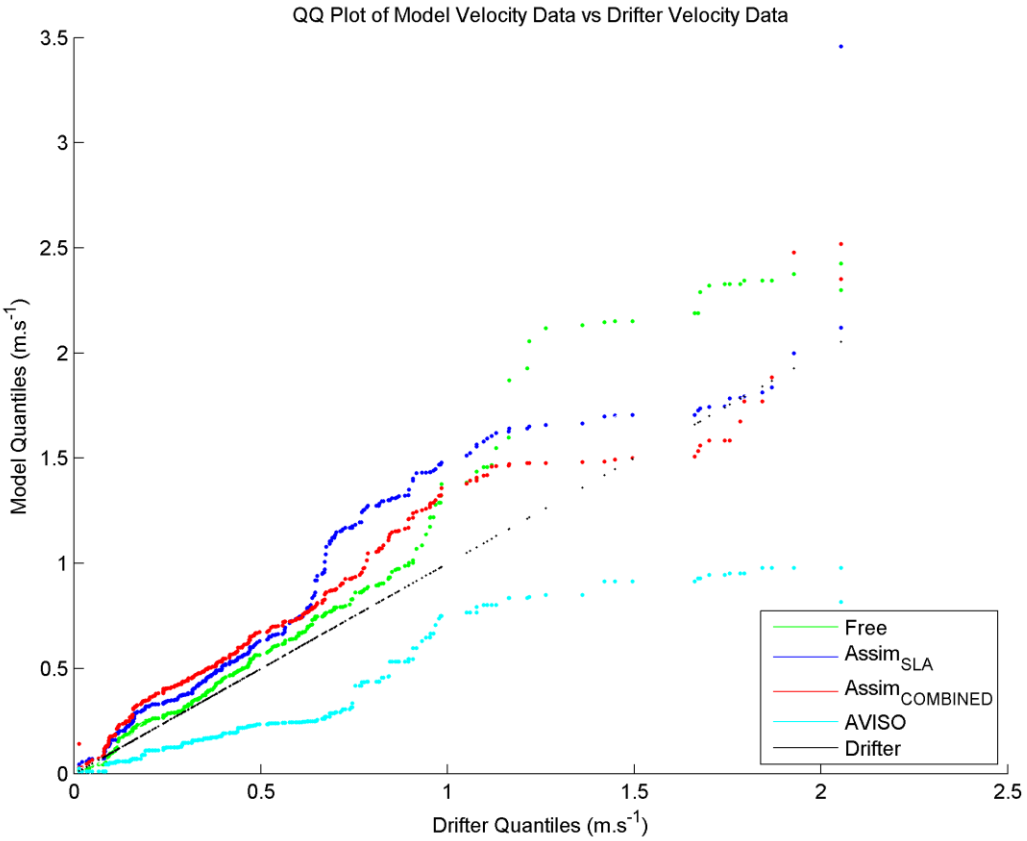

Figure 10 *Quantile-quantile (QQ) plot of the in situ drifter derived velocities compared to the modelled corresponding velocities. Illustrates how the modelled velocities compare to the in situ measurements.*

A correlation between the simulated (FREE, $ASSIM_{SLA}$ and $ASSIM_{COMBINED}$) and drifter-derived u and v component velocities was used as a proxy for the placement and timing in the region 26° – 36° S 22° – 34° E. An improvement in the correlation of $ASSIM_{COMBINED}$ (0.41) over $ASSIM_{SLA}$ (0.36) and FREE (0.06) is noted, further confirming that the combined SST-SLA assimilation has improved the models ability to correctly place mesoscale features in space and time in the Agulhas Current. Comparing the RMSE showed an improvement in $ASSIM_{COMBINED}$ (0.46) over $ASSIM_{SLA}$ (0.53) and FREE (0.63). This illustrates a significant improvement in the accuracy of the combined assimilation and suggests that the additional assimilation of SST is beneficial along the Agulhas Current. However, over the larger domain as seen earlier, there has been a decrease in accuracy.

$ASSIM_{COMBINED}$ has not appeared to have any big improvements/changes around the retroflection region, with only small pockets of changes on the order of 0.1 m/s present. However there appears to be a stronger eastward flow from retroflection to Agulhas Return Current, suggesting a slight improvement of the Agulhas Return Current located between 36° – 39° S and 16° -28° E. Many of the differences seem to be the result of the small-scale filaments being resolved in $ASSIM_{COMBINED}$.

Reproducing the Agulhas Return Current was one of the shortfalls in the previous study, and from this figure assimilating SST has been unable to improve upon this significantly, despite some marginal improvements in the retroflection region. In fact, velocities along the return current are lower in $ASSIM_{COMBINED}$ than $ASSIM_{SLA}$, degrading the representation of the current.

4.1.2. Subsurface velocities

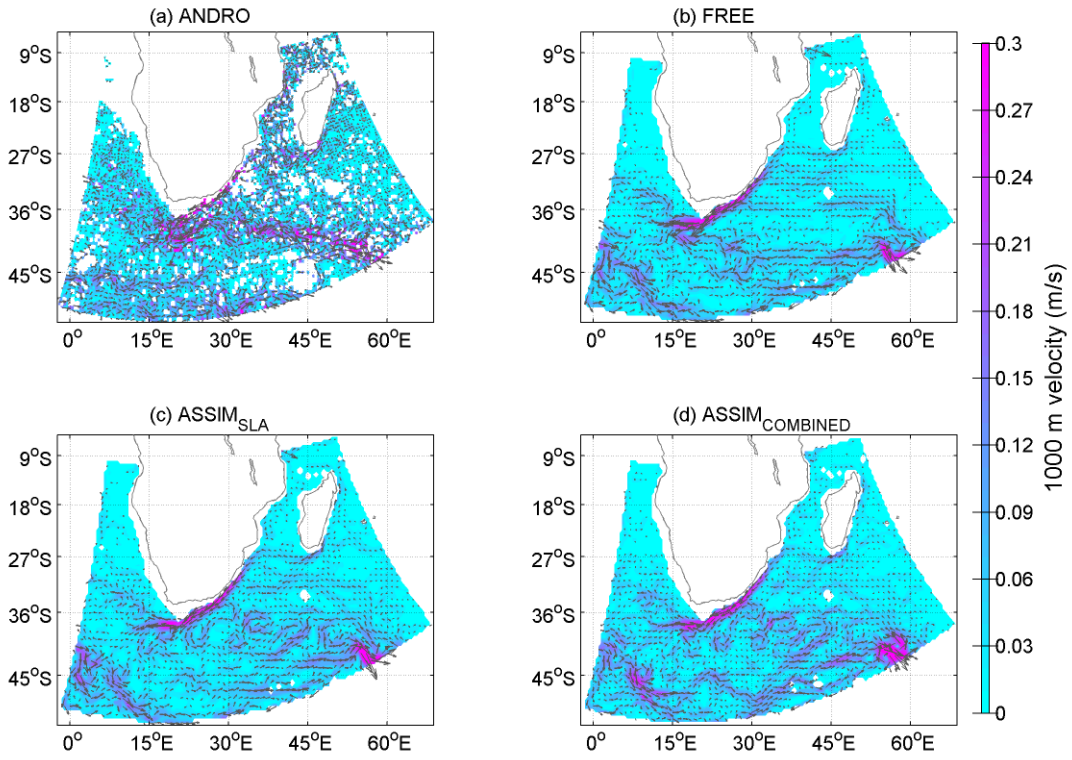

Figure 11 *1,000 m velocities from (a) the ANDRO Atlas, (b) FREE, (c) $ASSIM_{SLA}$, and (d) $ASSIM_{COMBINED}$.*

The spatial mean velocities from the ANDRO atlas (Ollitrault and Rannou, 2013) were gridded to a 0.1° grid, as were the 1,000 m velocities from the models (Fig.11). From the comparison (Fig.11), the most visible feature is that the assimilation of SST data seems to have improved the distribution pattern of the 1000 m velocities in the Southern Ocean, as well as the magnitude of velocity in the area. The Agulhas Return Current in $ASSIM_{COMBINED}$ remains too discontinuous, though the strength of the current has increased, it is still lower than that suggested by the ANDRO atlas. To quantify the results vector and linear correlations were done, along with RMSE and bias free RMSE ($RMSE_{bias\ free}$) calculations. The 1,000 m velocities in $ASSIM_{COMBINED}$ are an improvement over FREE, however, statistically, marginally worse than $ASSIM_{SLA}$. The difference in RMSE and $RMSE_{bias\ free}$ between $ASSIM_{COMBINED}$ and $ASSIM_{SLA}$ are not statistically significant, while they are both an improvement over

FREE. The changes from assimilating SST to the subsurface velocities are statistically negligible, however there is a noticeable improvement in the pattern of velocities in $ASSIM_{COMBINED}$.

Table 3 *Correlation (R) of the u and v component 1,000 m velocities, RMSE and bias free RMSE of the 1,000 m velocity magnitudes calculated against the ANDRO Atlas data set.*

	FREE	**$ASSIM_{SLA}$**	**$ASSIM_{COMBINED}$**
R_{linear}	0.33	0.39	0.37
$R_{u\ \&\ v\ comp.}$	0.18	0.20	0.17
RMSE	0.065	0.061	0.062
$RMSE_{bias\ free}$	0.0043	0.0038	0.0039

4.2. Surface Eddy Kinetic Energies

Eddy kinetic energy (EKE) is a crucial variable when it comes to the validation of an ocean modelling and data assimilation system (Backeberg et al., 2014). It is a proxy for mesoscale variability, can provide a spatial overview, highlighting regions of high and low mesoscale variability.

In Section 4.1.1, the surface velocities used were derived from drifter positions for 2008 and 2009. They were used to quantify the changes in the positioning and timing of mesoscale features; only 115 drifters entered the domain during that period. Unfortunately, the spatial coverage of the drifter data during this study period is too limited to provide a clear representation of the spatial distribution of surface eddy kinetic energy (EKE) in region. To calculate the mean surface EKE in the region (Fig.12), all data from every drifter entering the region since 1986, a total of 1,246 drifters, was used. The *u* and *v* velocity components are derived from the 6 h drifter positions and are then regridded daily to 0.1° over the HYCOM grid. These gridded velocities are then used to calculate mean surface EKE:

$$EKE = \frac{u'^2 + v'^2}{2}$$

Where $u' = u_{daily} - \bar{u}$ and $v' = v_{daily} - \bar{v}$, and $\bar{u}$, $\bar{v}$ are the mean for all the daily gridded *u* and *v* velocity components from 1986 to 2012.

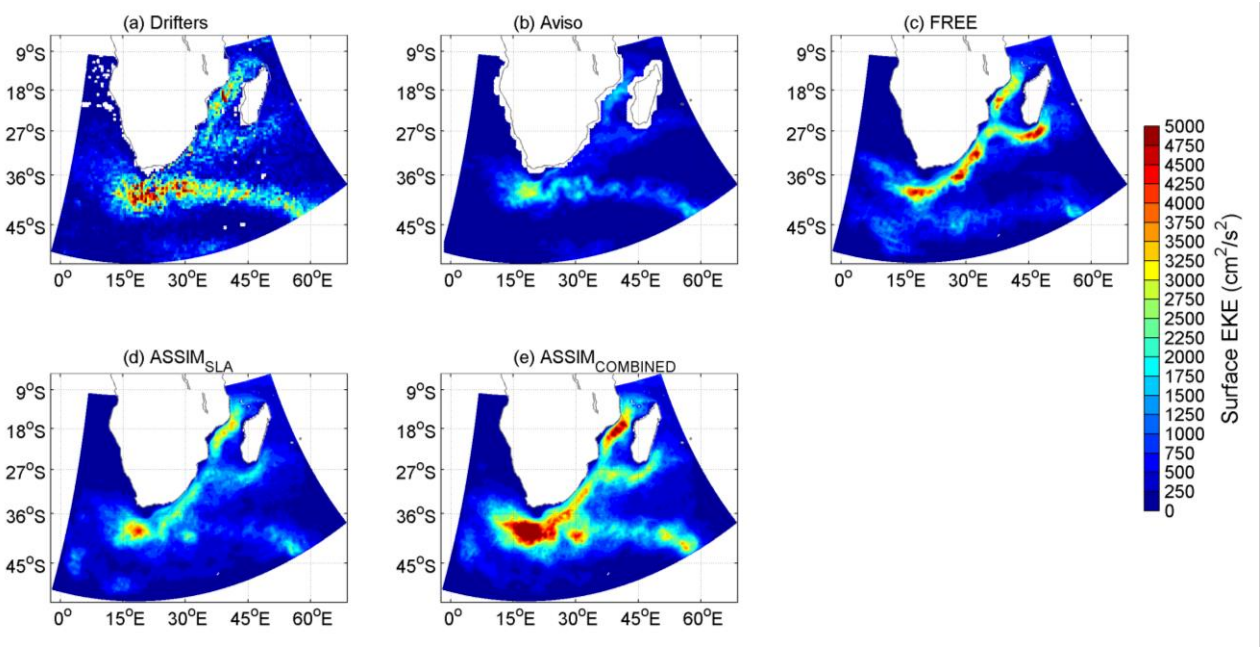

Figure 12 *Mean surface eddy kinetic energy (cm^2/s^2) derived from surface velocities of* ***(a)*** *the drifter data,* ***(b)*** *AVISO,* ***(c)*** *ASSIM$_{SLA}$,* ***(d)*** *FREE, and* ***(e)*** *ASSIM$_{COMBINED}$.*

In general, the spatial distribution of surface EKE in ASSIM$_{COMBINED}$ is more comparable with the drifter derived EKE, as opposed to ASSIM$_{SLA}$ and FREE. This improvement can be quantified by looking at the vector correlation (Table 4), there is an improvement in ASSIM$_{COMBINED}$. The assimilated models perform significantly better than the free run. However, even though the pattern and distribution of surface EKE in AVISO appears to be more in accordance to the drifter representation, it fails to accurately capture the correct levels of energy, underestimating it by a factor of 2 per the previous study by Backeberg et al., (2014).

After calculating the RMSE over the entire domain, it became evident that ASSIM$_{SLA}$ more accurately reproduces the surface EKE than ASSIM$_{COMBINED}$, FREE, and AVISO (Table 4). ASSIM$_{COMBINED}$ produces excessive levels of EKE within the retroflection, caused predominantly by the increase in the mean bias shown in section 4.1.1.

Table 4 *RMSE (cm^2/s^2) and vector correlation of eddy kinetic energy in the Agulhas Current system.*

	FREE	***ASSIM$_{SLA}$***	***ASSIM$_{COMBINED}$***	***AVISO***
RMSE	845.62	621.78	742.34	694.79
R$_{u\ \&\ v\ comp}$	0.49	0.71	0.76	0.79

The surface EKE results differ regionally. In the Mozambique Channel, surface EKE is over-estimated in ASSIM$_{COMBINED}$, with FREE representing the surface EKE here the best; ASSIM$_{SLA}$ and AVISO have

slightly lower surface EKE compared to the drifters in the area. In contrast, south of Madagascar, the excessively high levels of surface EKE present in FREE are reduced in both assimilations, however $ASSIM_{COMBINED}$ has higher surface EKE levels than the drifter field, while $ASSIM_{SLA}$ provides the most realistic levels, with AVISO underestimating the surface EKE.

Offshore of the Agulhas Current, the exaggerated levels of surface EKE, extending from 30°S to the retroflection, present in FREE are reduced again in both assimilations, with the $ASSIM_{COMBINED}$ continuing to overestimate the surface EKE. Compared to the drifters and AVISO, both assimilations produce surface EKE fields that are too high. AVISO provides the most realistic representation of surface EKE in this area, while $ASSIM_{SLA}$ performs the best among the model runs. This pattern of high EKE offshore of the Agulhas Current core in FREE and $ASSIM_{COMBINED}$ is caused by frequent eddies forming and propagating consistently along the same pathway from the Agulhas Current source regions to the retroflection, a reason stated in the previous study (Backeberg et al., 2014); this is a well noted common deficiency of model simulations of the Agulhas Current (Penven et al., 2010).

The surface EKE spatial distribution around the Agulhas retroflection region in $ASSIM_{COMBINED}$ produces a better comparison with the drifter observations and AVISO, in comparison to $ASSIM_{SLA}$ and FREE. However, the levels of surface EKE in $ASSIM_{COMBINED}$ are excessively high, and cover a larger area in the retroflection relative to drifter observations. The spatial expansion of surface EKE into the South Atlantic Ocean is larger, stretches further west, and is more in line with the drifter observations in $ASSIM_{COMBINED}$ than in $ASSIM_{SLA}$. The preference for eddies to follow a confined and narrow trajectory present in FREE is improved through the assimilation, in both $ASSIM_{SLA}$ and $ASSIM_{COMBINED}$, with the latter providing a better representation of the trajectory pathways.

In FREE, the surface EKE that is generally represented by the variability in the Agulhas Return Current is absent, highlighting the free running models inability to reproduce the return flow (Backeberg et al., 2014). In $ASSIM_{SLA}$ the position of the Return Current is somewhat more realistic, however, signs of the current disappear very sharply when moving eastward and the levels of surface EKE in the region are still lower than those recorded by drifter observations and AVISO. These limitations, presented in the previous study, have been improved upon in $ASSIM_{COMBINED}$. The position of the Return Current remains realistic and the levels of surface EKE resemble the drifter observations more closely, although being in excess, and do a better job representing the geographic pattern of surface EKE in the area than that of AVISO.

The AVISO surface EKE is lower than the surface EKE determined from drifter observations (Fig.12), particularly in regions of high mesoscale variability such as the retroflection. This was also shown in the previous study by Backeberg et al., (2014). High levels of surface EKE represented in the drifter

observations can be accounted for by the fact that the drifter observations record both the geostrophic and ageostrophic components of the current, as well as small scale features in the lagrangian flow, while altimetry measurements are only able to capture the eulerian geostrophic component (Backeberg et al., 2014). It is therefore encouraging that both $ASSIM_{COMBINED}$ and $ASSIM_{SLA}$, as well FREE could produce more realistic levels of surface EKE compared to AVISO. The assimilation of SST has certainly improved the spatial distribution of EKE, however, in most areas like the Retroflection region and offshore of Agulhas Current, surface EKE levels are too high compared to the drifter fields. This needs to be looked at in the future.

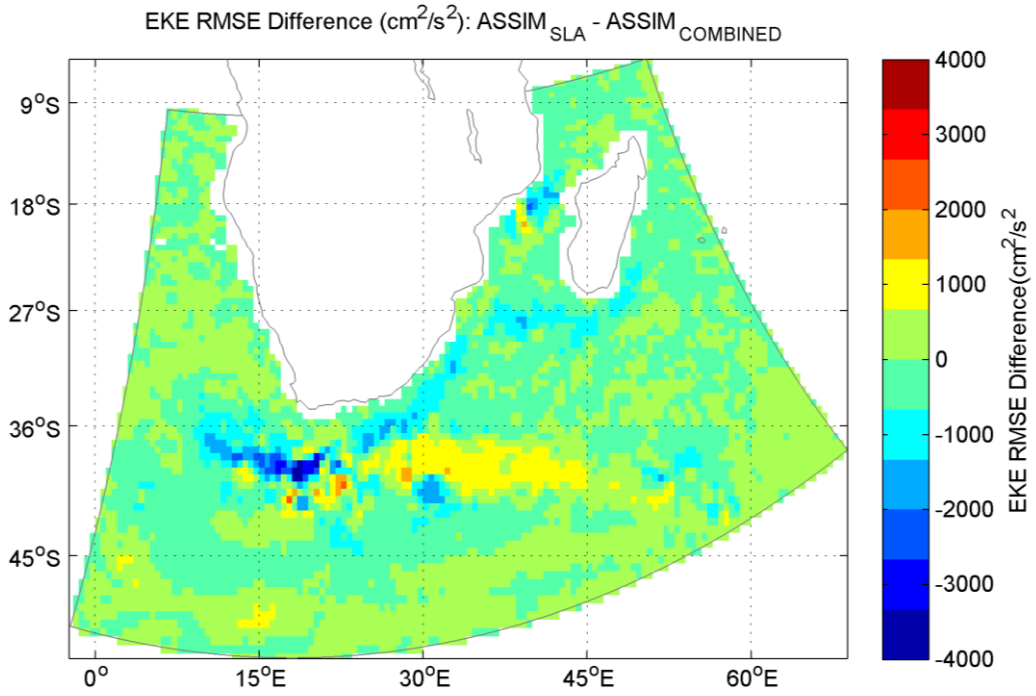

Figure 13 *RMSE surface EKE difference plot between $ASSIM_{SLA}$ and $ASSIM_{COMBINED}$, highlights areas where $ASSIM_{COMBINED}$ has improved, red, or worsened, blue.*

Examining the RMSE (Fig.13), the results are once again varied. It appears that assimilating SSTs has had both a negative and positive impact on the accuracy of the model compared to drifter derived EKE, depending on the location. The total RMSE over the entire region has increased in $ASSIM_{COMBINED}$ (Table 4), the RMSE is now higher than that of $ASSIM_{SLA}$ and AVISO. This is largely due to excessively high surface EKE levels in areas of large mesoscale variability, the Retroflection (Fig. 13), and the slightly elevated surface EKE levels in the Mozambique Channel, south of Madagascar, and along the Agulhas Current, where too frequent eddy production is the likely cause. $ASSIM_{COMBINED}$ has however improved surface EKE RMSE significantly along the Return Current (Fig.13), as well as slightly improving the levels of surface EKE across some areas of the Southern Ocean. This highlights the varied

performance of $ASSIM_{COMBINED}$ and suggests that the model needs further work an improvement. On the other hand, AVISO underestimates the surface EKE in the region, but has better timing and positioning of features, this highlights the benefit of combining both a high resolution dynamical model and altimetry observations, which was also stated by Backeberg et al., (2014).

4.3. Sea Surface Temperatures

OSTIA SST satellite data was used to validate the models skill at reproducing SSTs. These daily OSTIA SST data sets were regridded daily to the HYCOM 0.1° grid, the gridded SSTs were then averaged over the two-year study period, 2008 - 2009, to create a mean SST map.

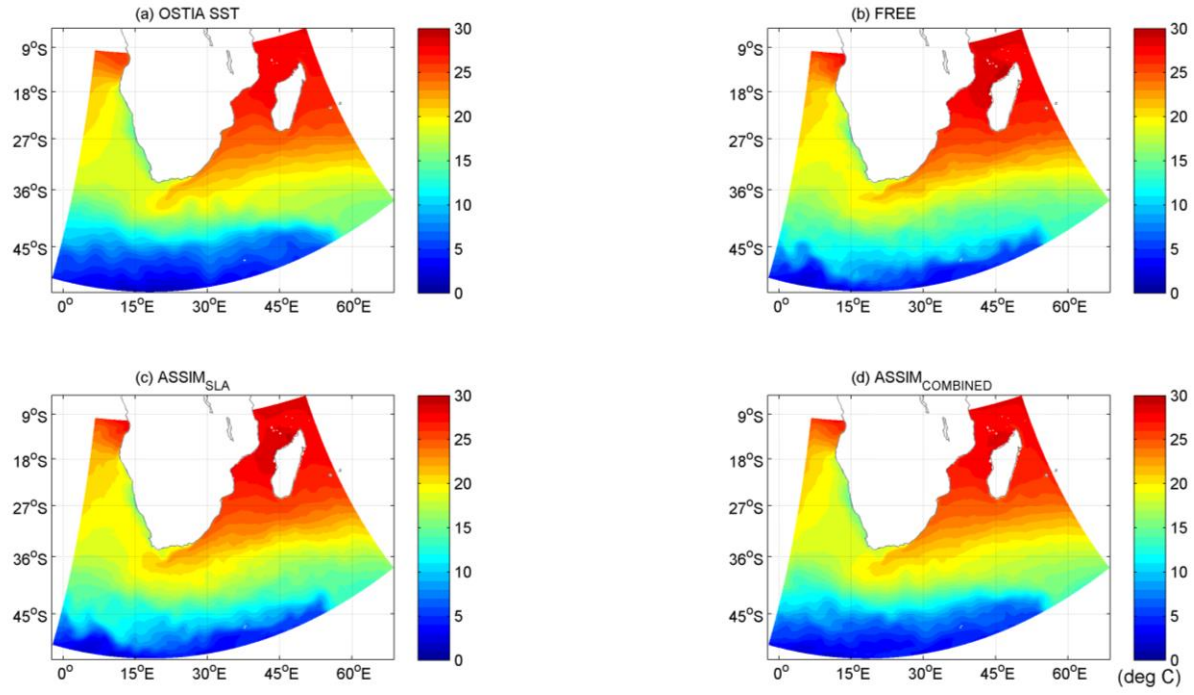

Figure 14 *Mean sea surface temperatures (◦C) from* ***(a)*** *the OSTIA data,* ***(b)*** *FREE,* ***(c)*** *$ASSIM_{SLA}$, and* ***(d)*** *$ASSIM_{COMBINED}$.*

In the $ASSIM_{SLA}$ and FREE there is an area of 28 - 29° C (Fig.14) water, towards the north of Madagascar, not present in OSTIA; assimilating SST has removed this feature in $ASSIM_{COMBINED}$. The spatial representation of the Retroflection in $ASSIM_{COMBINED}$ is more in line with that of the OSTIA fields, an improvement over FREE and $ASSIM_{SLA}$. The spatial representation of the Southern Ocean (Fig.14) has also improved over FREE and $ASSIM_{SLA}$, the colder 5° C water is distributed further north in $ASSIM_{COMBINED}$; resembling that of the OSTIA observations. The flow of warmer 20° C waters into the South Atlantic from the Retroflection, is in closer agreement with that of the OSTIA representation. The band of West Coast upwelling, 12 - 13° C water, has become slightly broader, and spreads further north, more indicative of the observations. The spatial representation of colder 16° C waters, associated with the northward meander of the Agulhas Return Current as it flows around the Agulhas

Plateau near 40° S 25° E, appears to have improved in $ASSIM_{COMBINED}$, an improvement over $ASSIM_{SLA}$. The area of 20° C water from the Retroflection to the Cape Basin in $ASSIM_{SLA}$ and FREE, resulting from the movement of eddies into the South Atlantic, has been removed in $ASSIM_{COMBINED}$, resembling the SST field of OSTIA. Overall, $ASSIM_{COMBINED}$ appears to provide a more realistic representation of the region, based on OSTIA representation, when compared to the $ASSIM_{SLA}$ and FREE.

From Fig.15, a difference plot of SST between OSTIA and $ASSIM_{SLA,}$ the biggest changes are evident in the Southern Ocean, along the west coast upwelling region, and at the south-eastern corner of the domain. $ASSIM_{SLA}$ is up to 3 ° C warmer than OSTIA over most of the Southern Ocean, it is 1-2 ° C warmer along the west coast upwelling zone, and it is 1-3 ° C warmer than OSTIA in the south-eastern corner of the domain.

When looking at Fig.16, difference plot of SST between OSTIA and $ASSIM_{COMBINED}$, the improvement of assimilating SST can be clearly seen. The differences between OSTIA and $ASSIM_{COMBINED}$ are minimal; the only significant differences being centred on the Southern Ocean, with $ASSIM_{COMBINED}$ being up to 3 - 4 ° C warmer in some small areas. The improvement is further illustrated when calculating the RMSE. The RMSE for all SST data was calculated over all forecast cycles for 2008 and 2009. In this case, the mean RMSE is significantly lower in $ASSIM_{COMBINED}$ (0.46 ° C) compared to $ASSIM_{SLA}$ (1.57 ° C), and FREE (1.44 ° C); highlighting the significant improvement in the accuracy of the combined assimilations SST field. This was one of the major limitations in the previous study, where the assimilation of SLA led to a degradation of the SST fields in the model, leading to larger error in the assimilation over the free running model. This is a positive improvement, as it appears that the assimilation of SST has successfully restored the SST field in the model, as well as improving the result; reducing the error quite noticeably.

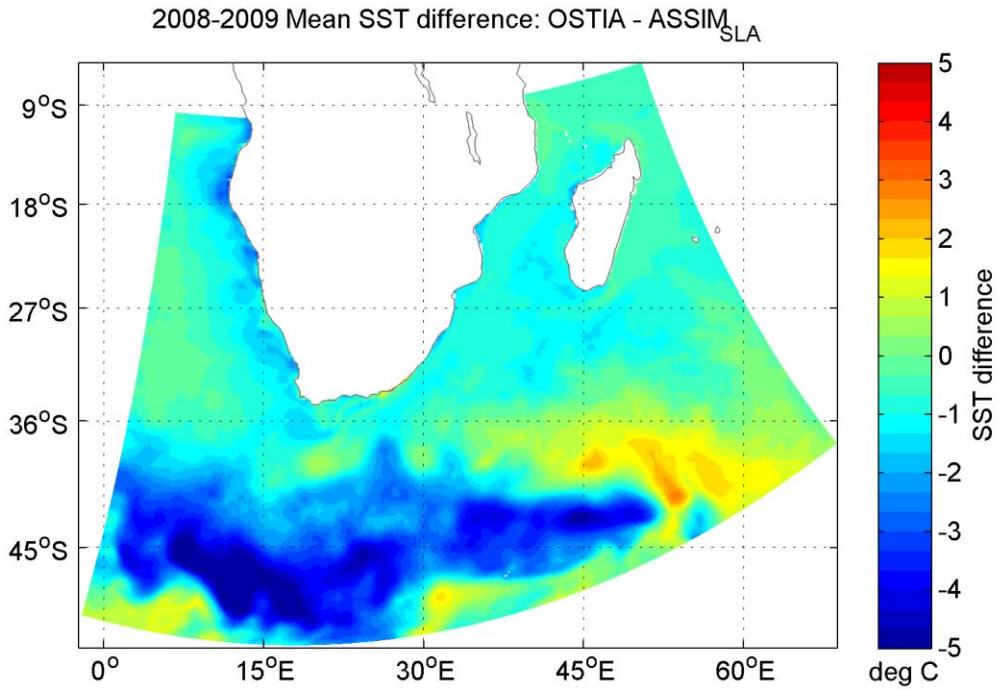

Figure 15 *Spatial Mean SST difference (◦C) plot, calculated between OSTIA and ASSIM$_{SLA}$. Highlights where ASSIM$_{SLA}$ overestimates or underestimates SST.*

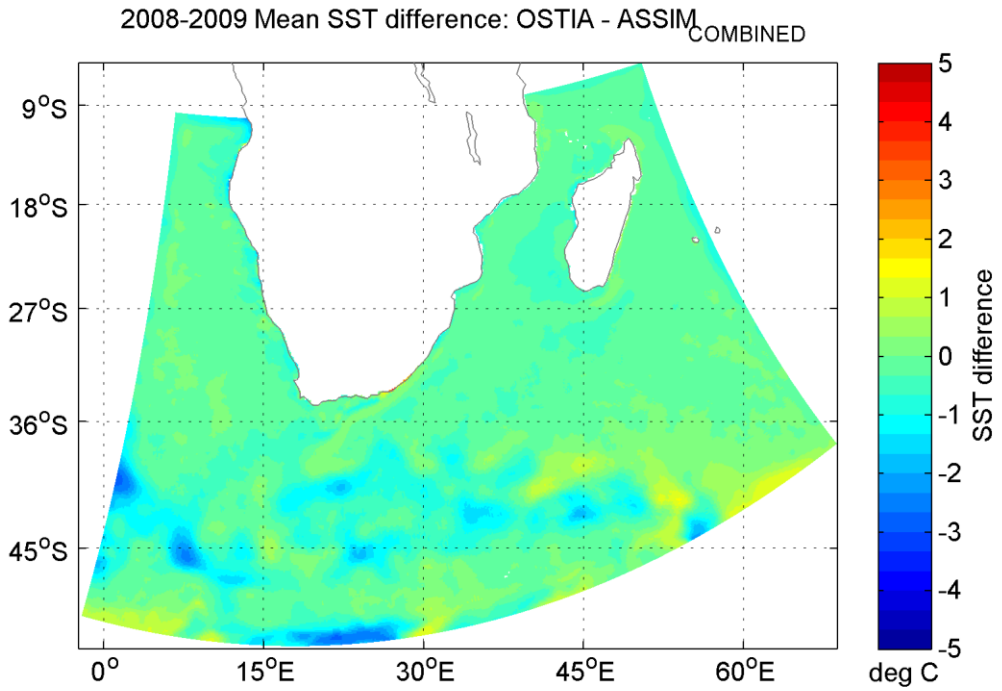

Figure 16 *Spatial Mean SST difference (◦C) plot, calculated between OSTIA and ASSIM$_{COMBINED}$. Highlights where ASSIM$_{COMBINED}$ overestimates or underestimates SST.*

As mentioned previously, the numerical model had a large SSH bias in the Agulhas Current System (Backeberg et al., 2014). The incorrect mean in the area resulted in poorly resolved dynamics in the free-running HYCOM, which in turn resulted in an incorrect multivariate correlation during the $ASSIM_{SLA}$ assimilation. As can be seen in Fig.17 below, the FREE correlation map illustrates incorrect correlation in the FREE model, particularly in the Southern Ocean region. There is a large positive bias of the SST-SSH correlation in the Southern Ocean, and the general spatial representation of the correlations are inconsistent with the observed map. This bias in the Southern Ocean appears to have been removed in $ASSIM_{SLA}$ however there is now a weak correlation lower than observed (Fig.17). The spatial distribution of the correlations in $ASSIM_{SLA}$ are slightly more consistent with the observed, despite the levels being significantly lower. These lower correlation levels are thought to be due to the SST degradation, which was caused by the assimilation of SLA. Assimilating SST into the model corrected the SST degradation and in turn appears to have made a significant improvement on the correlations (Fig.17). The bias in the Southern Ocean present in FREE has been corrected and the low levels in $ASSIM_{SLA}$ have also been improved upon in $ASSIM_{COMBINED}$. The spatial distribution has also seen an improvement, and looking at Fig.18 it is noticeable that the large differences between the observations and $ASSIM_{COMBINED}$ fall around the boundaries. The correlation differences over the Agulhas Current System are minimal, falling within 0.2 either side of zero (Fig.18). There are two noticeable spots within the Agulhas Current System when the difference is larger; inshore of the Agulhas Current, south of Port Elizabeth, and at the southern tip of the Agulhas Bank, in the retroflection. Here the correlation is exaggerated by up to 0.8, with the observations displaying an anti-correlation between SST and SSH in these areas, while $ASSIM_{COMBINED}$ shows a weak correlation.

To illustrate the improvement of the relationship between SST and SSH, time-series plots and correlations were calculated for the point located at 37.81^{o} S 28.48^{o} E (Fig.19). This point was chosen as an example to highlight the improved co-varying relationship between SST and SSH. From these time-series it is noticeable how good SST and SSH now vary with respect to one another as compared to FREE, $ASSIM_{SLA}$ and the observations (Fig.19). The correlations quantitatively show the improvement (Observation = 0.62, FREE = 0.54, $ASSIM_{SLA}$ = -0.19, $ASSIM_{COMBINED}$ = 0.65). $ASSIM_{COMBINED}$ slightly over-estimates the correlation compared to the observed, however it is a significant improvement over $ASSIM_{SLA}$ which suggested an anti-correlation in the area contrary to observations, and FREE which underestimated the correlation. The time-series and correlations show the improved performance of $ASSIM_{COMBINED}$ in this example area, and the same can be seen in other areas where the additional SST assimilation has improved the SST-SSH correlations (Fig.17 and Fig.18).

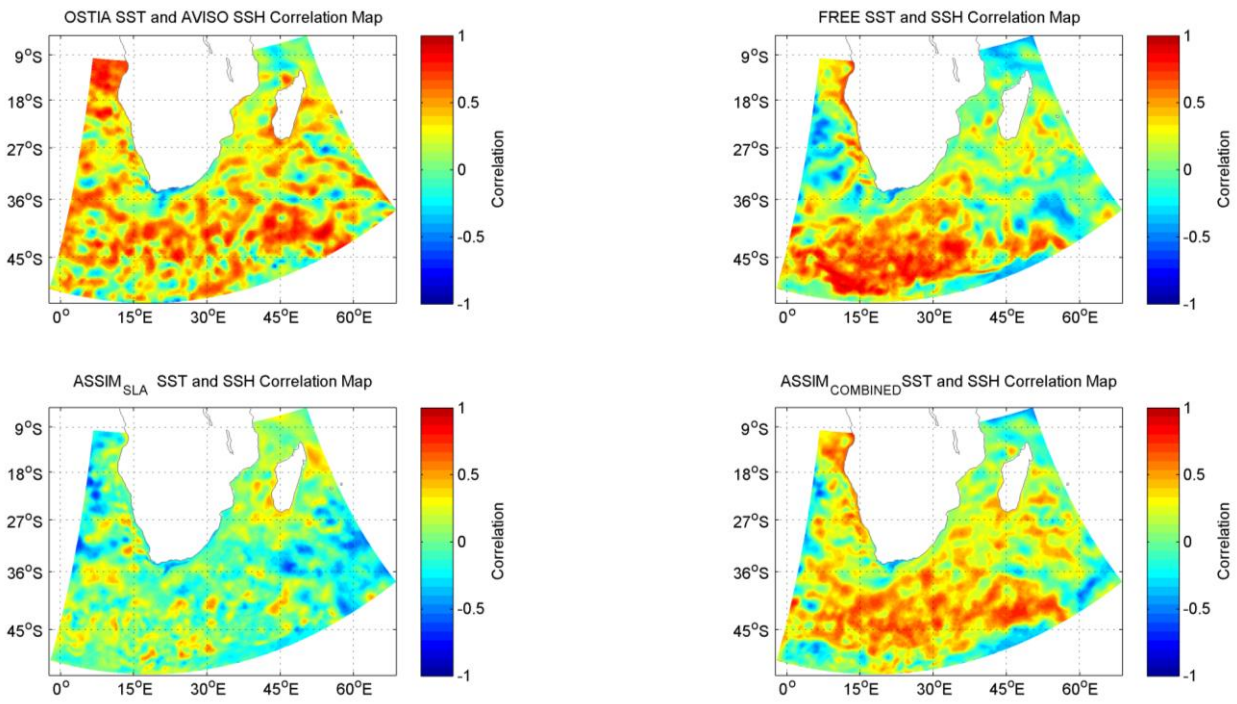

Figure 17 *Correlation maps of SST and SSH for the period 2008 – 2009. Illustrates the relationship between SST and SSH, as well as how well the models replicate that relationship.*

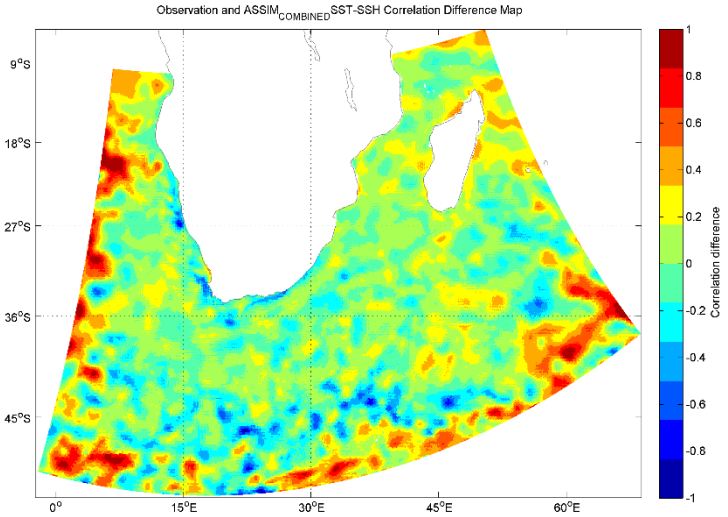

Figure 18 *Map showing the differences between the correlations for SST-SSH in the observed data and ASSIM$_{COMBINED}$. Areas in red are where the model underestimates the correlation and blue areas are where the model over-estimates the correlation.*

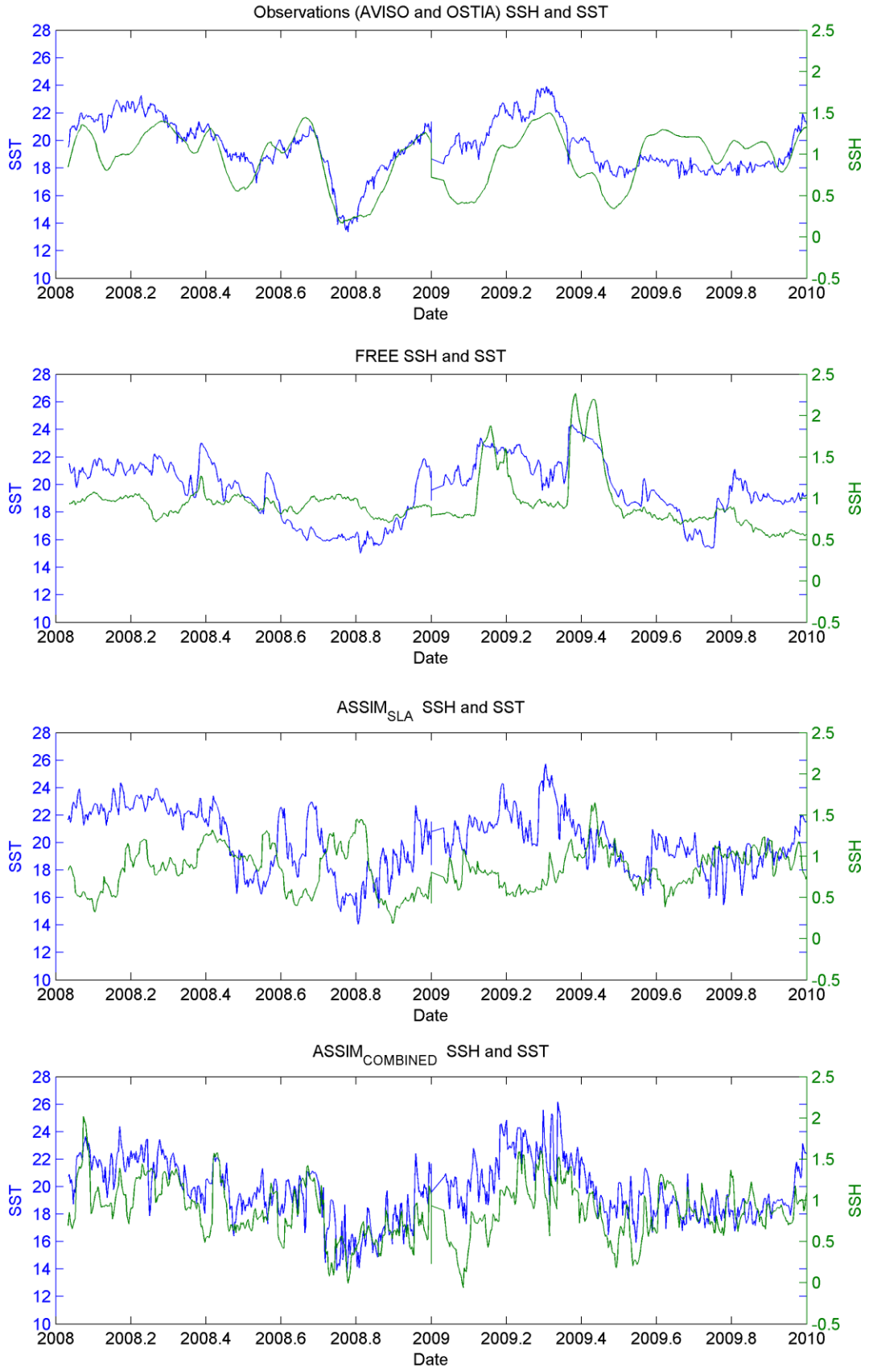

Figure 19 *Time-series plots of SST and SSH for the location 37.81º S 28.48º E; for the observations (AVISO and OSTIA), FREE, ASSIM$_{SLA}$ and ASSIM$_{COMBINED}$.*

The assimilation of SST has corrected the SST degradation induced through the SLA assimilation and improved the spatial representation and accuracy of the models SST fields. Assimilating SST has also improved the correlation between SSH and SST, the levels of correlation measured and the spatial distribution are now more in-line with the observations compared to the previous model runs.

4.4. T/S profiles

Using all available Argo profiles in the region for the period 2008 – 2009, mean temperature-salinity (T/S) profiles were then calculated for the entire Agulhas Current System (15° – 45° E, 12° – 45° S), the Agulhas Current core (23° – 33° E, 27° – 36° S), the Agulhas Retroflection (15 ° – 22° E, 36° – 43° S) and the Agulhas Return Current (23° – 43° E, 36° – 43° S; (Fig.19).

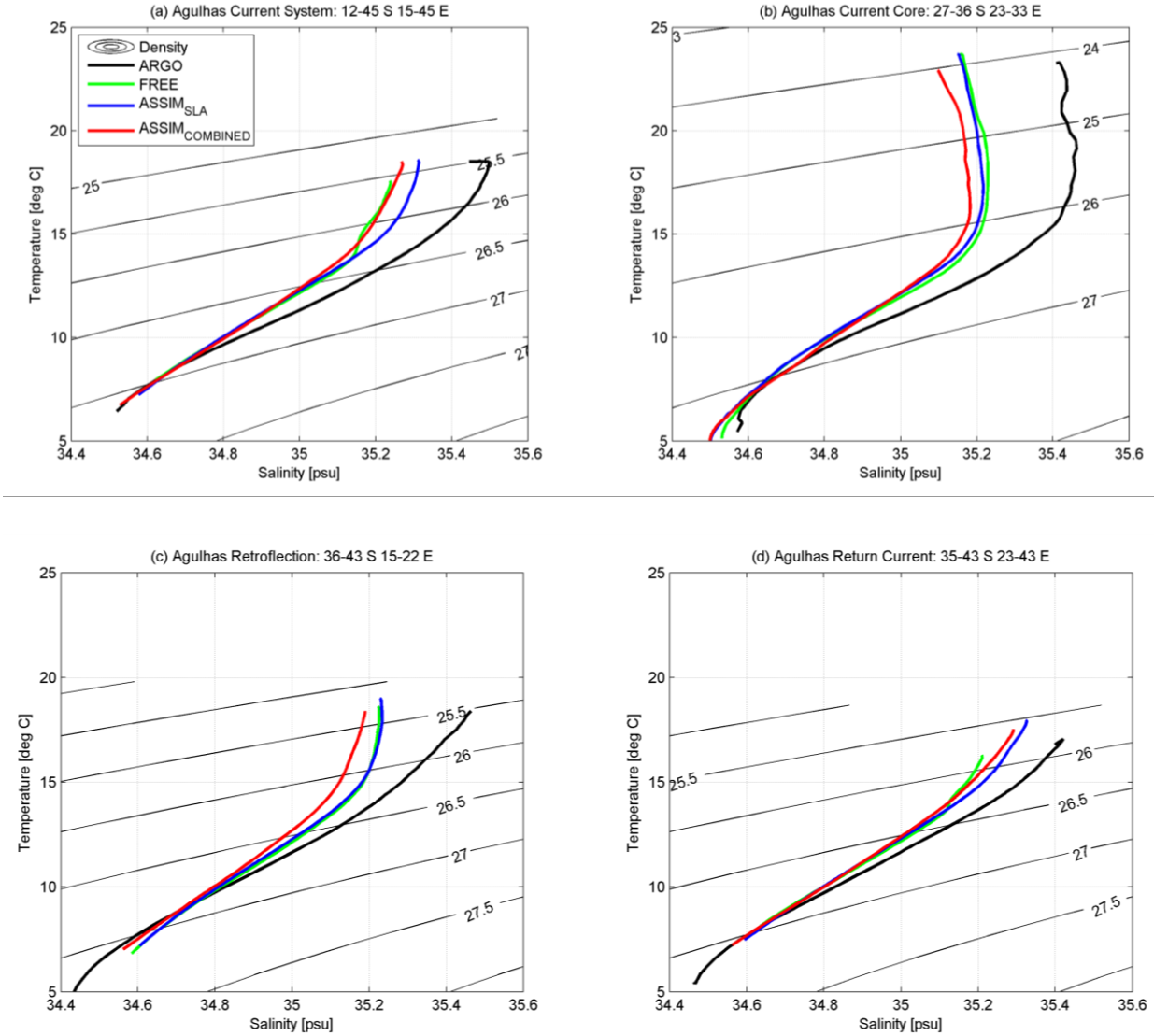

Figure 19 *Mean temperature–salinity diagrams from all Argo profiles for 2008–2009. (a) Averaged for the greater Agulhas Current System (12 – 45 S 15 – 45 E), (b) the Agulhas Current core (27 - 36 S 23 – 33 E), (c) the Agulhas Retroflection (36 – 43 S 15 – 22 E), and (d) the Agulhas Return Current (35 – 43 S 23 – 43 E).*

Across the entire Agulhas Current system, it is evident that assimilating SST data has a negative impact on water masses in the range of $T > 15^{o}$ C and $S > 35.1$ PSU, freshening these with respect to the observed Argo profiles. When looking at the different regions of the Agulhas Current system, the smallest water mass change associated with the assimilation occurs in the Agulhas Return Current, where surface temperatures are improved, however the profile is still more anomalous than $ASSIM_{SLA}$ with respect to from the Argo profile, and salinity is still underestimated, a trend noticeable in all the profiled regions. In all the profiled regions, $ASSIM_{COMBINED}$ has a negative salinity bias, which indicates that the salinity in the upper 500 m is underestimated. Surface salinities in the Agulhas core (Fig.19b) and in the Retroflection (Fig.19c), are severely underestimated by $ASSIM_{COMBINED}$, performing worse than the FREE in these areas. Over the whole Agulhas System, $ASSIM_{COMBINED}$ performs about the same as the FREE, and worse than $ASSIM_{SLA}$ in the upper ocean. Only at the surface has it improved surface temperatures over FREE.

While the assimilation of SST has improved the surface temperatures, it has not been able to improve upon the negative salinity bias throughout the water column. This bias has been enhanced with the inclusion of SST in the assimilation, this could be due to the model adjusting this variable to satisfy the constraints of the assimilation. When one observation is assimilated, the model is constrained so that it satisfies the solution of the assimilated observation. When two or more observations are assimilated, the skill of the model should improve, but only if it were a perfect model; this is not the case. When a model is imperfect the true state may prove to be unsustainable by the model. The assimilation method thereby attempts to find a solution that satisfies all the observations assimilated, a best of both worlds, compromised solution. By doing this it is not unexpected to see a degradation of variables when multiple observations are assimilated. The degradation can become quite severe for variables which are unobserved/unconstrained, as the assimilation method will freely adjust these variables to satisfy the assimilated observations. Subsurface salinity, and less so subsurface temperatures, have been degraded due to these adjustments, and these assimilation adjustments are part of the reason for the negative salinity bias. The assimilation of T/S hydrographic profiles in the future could improve this aspect.

These T/S plots illustrate the models limitations with regards to reproducing subsurface fields. It is vital that assimilation improves the representation of subsurface dynamics and features, as one of the biggest bonuses of an assimilation system is that it allows for the study of subsurface oceanography; as satellites are limited to the ocean surface, and cannot give us a view of the inner ocean. Future work should look at ways to improve the subsurface modelling capability, possibly through the assimilation of subsurface observations or the parameterization of subsurface variables; to limit the models adjustment of these unobserved variables.

5. Summary and Outlook

This data assimilation experiment focused on the impacts of assimilating SST, along with along-track SLA into a HYCOM model of the Agulhas region. The influence of the assimilation on the model was assessed by comparing the SST and SLA assimilated run against an SLA-only assimilated run, an unassimilated run, satellite observed SST, from OSTIA, and persistence forecasts from satellite altimetry observations, from AVISO. The surface drifter observations, and Argo float measurements were used to quantify the differences between the models, OSTIA and AVISO.

The assimilation of SST along with SLA into the HYCOM model has had a mixed impact in terms of accuracy of the model when compared to $ASSIM_{SLA}$. The correlation between the *u* and *v* velocity components, used as a proxy for the positioning and progression of mesoscale features, was slightly improved in $ASSIM_{COMBINED}$ compared to $ASSIM_{SLA}$. However, the RMSE of surface velocities has increased in $ASSIM_{COMBINED}$. While $ASSIM_{COMBINED}$ can better capture the positioning and timing of these mesoscale features, it cannot capture their magnitude as well as $ASSIM_{SLA}$, with a decrease in accuracy when analysing the entire domain. The differences between the mean velocity fields of $ASSIM_{SLA}$ and $ASSIM_{COMBINED}$ are most noticeable along the Agulhas Current and in the Southern Ocean, with the assimilation of SST appearing to have improved the accuracy of mean velocities over the Agulhas Current. However, both assimilations are unable to perform as accurately as AVISO over the entire region. The assimilation has had mixed results on the surface velocities, with noticeable improvements in the smaller area over the Agulhas Current, and to the spatial distribution of mesoscale and sub-mesoscale variability.

When looking at the regional surface EKE, $ASSIM_{COMBINED}$ is not as accurate as $ASSIM_{SLA}$ or AVISO at producing the correct levels of energy, tending to overestimate surface EKE. However, compared to $ASSIM_{SLA}$, $ASSIM_{COMBINED}$ has improved the spatial representation of surface EKE and is able to recreate the Agulhas Return Current. The surface EKEs in $ASSIM_{COMBINED}$ are however, exaggerated in high mesoscale variability regions, particularly the Agulhas Retroflection. This bias in areas of high variability is thought to be the main cause of the decrease in accuracy. The surface velocity bias is the likely reason for the surface EKE bias. Corrections to the underlying model numerics will need to be made, as assimilation does not appear to be the solution with regards to surface EKE and velocities.

Table 5 *Summary of correlations (R) and RMSE used in the validation.*

	FREE	**ASSIM$_{SLA}$**	**ASSIM$_{COMBINED}$**	**AVISO**
R$_{drifter\ u\ \&\ v\ comp.}$	0.07	0.33	0.35	0.91
RMSE$_{drifter\ vel.\ mag}$ (m/s)	0.31	0.26	0.30	0.18
RMSE$_{drifter\ EKE}$ (cm^2/s^2)	845.62	621.78	742.34	694.79
RMSE$_{OSTIA\ SST}$ (^oC)	1.44	1.57	0.46	
R$_{ANDRO\ u\ \&\ v\ comp.}$	0.18	0.20	0.17	
RMSE$_{ANDRO\ vel.\ mag.}$ (m/s)	0.065	0.061	0.0621	

One area where the assimilation of SST into the model was expected to have the biggest impact, was on the accuracy of SST in the model. ASSIM$_{COMBINED}$ has significantly improved the accuracy of the model with regards to the RMSE of OSTIA SSTs. The SST degradation produced by the assimilation of only SLA in ASSIM$_{SLA}$, has been rectified in ASSIM$_{COMBINED}$, with the spatial coverage and SST levels being well represented. The SST assimilation was also able to improve upon the SST-SSH correlation in the model. The spatial representation and levels of correlation in ASSIM$_{COMBINED}$ are more in line with that of the observed satellite correlations. ASSIM$_{COMBINED}$ has improved upon the Southern Ocean bias present in FREE, as well as the under representation of correlation in ASSIM SLA. The improvement of SSTs as well as SST-SSH correlations are the most promising results from this assimilation.

Satellites being unable to provide information on the interior of the ocean, model assimilations can be very useful to help resolve water masses and transports. Unfortunately, in this case, the assimilation of SST into the dynamical model has had a negative impact on the representation of water mass properties. While temperatures at the surface were improved, the negative salinity bias present in FREE and ASSIM$_{SLA}$ was enhanced or saw little change, resulting in water mass profiles that are too fresh. This bias could be rectified in the future by assimilating T/S profiles as well.

Visually, the spatial representation of 1000 m subsurface velocities, in ASSIM$_{COMBINED}$, improved, however statistically they appear to have worsened, looking at vector and linear correlations. The correlation of *u* and *v* components decreased, while the RMSE between model output and Argo-derived velocities increased compared to ASSIM$_{SLA}$. This again could be the result of the method of validation used as mentioned earlier. So, while ASSIM$_{SLA}$ provided a better statistical representation of the water mass properties and the 1000 m subsurface velocities, ASSIM$_{COMBINED}$ produced a better visual representation. None of the models could however reproduce the structure of the Agulhas

Return Current at 1000 m. T/S plots highlighted the need for T/S profiles to be assimilated into the model for improved performance.

Overall, the results appear promising, with the assimilation showing many improvements. Future work will focus on improving the dynamics of the free running model, from which the static ensemble is derived. The Agulhas Return Current at the surface and 1000 m, remains, statistically, poorly represented, and the salinity bias present in the water mass properties needs to be rectified. So, while the assimilation of SLA only, in Backeberg et al. (2014) highlighted the benefits of assimilation, the results of this study highlights the importance of having both accurate dynamics within the free running model as well assimilation. Assimilation can only improve a model to a certain extent, and in this study the limitations of assimilation have been shown.

6. References

Antonov JI, Locarnini RA, Boyer TP, Mishonov AV, Garcia HE (2006). World Ocean Atlas 2005, Volume 1: Salinity. p. 182 pp. NOAA Atlas NESDIS 61. U.S. Government Printing Office, Washington.

Backeberg BC, Johannessen JA, Bertino L, Reason CJ (2008). The greater Agulhas Current system: an integrated study of its mesoscale variability. J Oper Oceanogr 1(1):29–44.

Backeberg BC, Bertino L, Johannessen JA (2009). Evaluating two numerical advection schemes in HYCOM for eddy-resolving modelling of the Agulhas Current. Ocean Sci 5:173–190.

Backeberg BC, Johannessen JA, Rouault M, Veitch J (2010). Preliminary inter-model comparison of the Agulhas Current with direct range doppler velocity estimates from Envisats Advance Synthetic Aperture Radar In: Special Publication SP-686 on CD. Eurpean Space Agency, ESAs Publications Division (EPD).

Backeberg BC, Penven P, Rouault M (2012). Impact of intensified Indian Ocean winds on mesoscale variability in the Agulhas system. Nat Clim Chang 2:608–612.

Backeberg BC, Reason CJ (2010). A connection between the South Equatorial Current north of Madagascar and Mozambique Channel Eddies. Geophys Res Lett 37:L04604. doi:10.1029/2009GL041950.

Backeberg BC, Counillon F, Johannessen JA, Pujol MI (2014). Assimilating Along-track SLA data using the EnOI in an eddy resolving model of the Agulhas system. Ocean Dyn 64: 1121-1136.

Barnier B, Madec M, Pendruff T, Molines JM, Treguier AM, Sommer JL, Beckmann A, Biastoch A, Boning C, Dengg J, Derval C, Durand E, Gulev S, Remy E, Talandier C, Theetten S, Maltrud M, McClean J, DeCuevas B (2006). Impact of partial steps and momentum advection schemes in a global ocean circulation model at eddy permitting resolution. Ocean Dyn 56(5-6):543–567.

Beal LM, De Ruijter WPM, Biastoch A, Zahn R (2011). On the role of the Agulhas system in ocean circulation and climate. Nat 472:429–436.

Bentsen M, Evensen G, Drange H, Jenkins AD (1999). Coordinate transformation on a sphere using conformal mapping. Mon Weather Rev 127:2733–2740.

Biastoch A, Boning CW, Lutjeharms JRE (2008). Agulhas leakage dynamics affects decadal variability in Atlantic overturning circulation. Nat 456:489492.

Biastoch A, Boning CW, Schwarzkopf FU, Lutjeharms JRE (2009). Increase in Agulhas leakage due to poleward shift of Southern Hemisphere westerlies. Nat 462:495–498.

Biastoch A, Lutjeharms JRE, Boning CW, Scheinert M (2008). Mesoscale perturbations control inter-ocean exchange south of Africa. Geophys Res Lett 35:L20, 602.

Bleck R (2002). An oceanic general circulation model framed in hybrid isopycnic-Cartesian coordinates. Ocean Model 37:55–88.

Boebel O, Rossby T, Lutjeharms J.R.E, Zenk W, Barron C, (2002). Path and Variability of the Agulhas Return Current. Deep Sea Research. 50, 35-36.

Browning GL, Kreiss HO (1982). Initialization of the shallow water equations with open boundaries by the bounded derivative method. Tellus 34:334–351.

Browning GL, Kreiss HO (1986). Scaling and computation of smooth atmospheric motions. Tellus Ser A 38:295–313.

Bryden HL, Longworth HR, Cunningham SA (2005). Slowing of the Atlantic meridional overturning circulation at 25° N. Nature 438, 655-657; doi:10.1038/nature04385.

Byrne DA, McClean JL (2008). Sea level anomaly signals in the Agulhas Current region. Geophys Res Lett 35. doi:10.1029/2008GL034087.

Chelton DB, Deszoeke RA, Schlax MG, El Naggar K, Siwertz N (1998). Geographical variability of the first baroclinic Rossby radius of deformation. J Phys Oceanogr 28(3):433–460.

Counillon F, Bertino L (2009a). Ensemble Optimal Interpolation: Multivariate properties in the Gulf of Mexico. Tellus 61:296308.

Counillon F, Bertino L (2009b). High-resolution ensemble forecasting for the Gulf of Mexico eddies and fronts. Ocean Dyn 59:83–95.

Crosby DS, Breaker LC, Gemmill WH (1993). A proposed definition for vector correlation in geophysics: Theory and application. J Atmos Ocean Technol 10:355–367.

Daniault N, Menard, Y, (1985). Eddy kinetic energy distribution in the Southern Ocean from altimetry and FGGE drifting buoys. Journal of Geophysical Research. 90, 11877–11889.

Darbyshire J, (1972). The effect of bottom topography on the Agulhas Current. Pure Applied Geophysics. 101, 208–220.

Dee DP, Uppala SM, Simmons AJ, Berrisford P, Poli P, Kobayashi S, Andrae U, Balmaseda MA, Balsamo G, Bauer P, Bechtold P, Beljaars ACM, van de Berg L, Bidlot J, Bormann N, Delsol C, Dragani R, Fuentes M, Geer AJ, Haimberger L, Healy SB, Hersbach H, Holm EV, Isaksen L, Kallberg P, Kohler M, Matricardi

M, McNally AP, Monge-Sanz BM, Morcrette JJ, Park BK, Peubey C, de Rosnay P, Tavolato C, Thpaut JN, Vitart F (2011). The ERA-Interim reanalysis: Configuration and performance of the data assimilation system. Q J R Meteorol Soc 137(656):553–597. doi:10.1002/qj.828.

Dencausse G, Arhan M, Speich S, (2010). Spatio-temporal characteristics of the Agulhas Retroflection. Deep Sea Research Part 1: Oceanographic Research Papers. 57, 22, 1392-1405.

De Ruijter, W (1982). Asymptotic analysis of the Agulhas and Brazil Current systems, Journal of Physical Oceanography. 12, 361–373.

De Ruijter W.P.M, van Leeuwen J, Lutjeharms J.R.E, (1999). Generation and evolution of Natal Pulses: Solitary Meanders in the Agulhas Current. Journal of Physical Oceanography. 29, 3043-3055.

De Ruijter, W.P.M., H. Ridderinkhof, J.R.E. Lutjeharms, M.W. Schouten, and C. Veth, 2002. Observations of the flow in the Mozambique Channel. *Geophysical Research Letters*, **29**, 140.1-140.3.

Dibarboure G, Pujol MI, Briol F, Traon PYL, Larnicol G, Picot N, Mertz F, Ablain M (2011). Jason-2 in DUACS: Updated system description, first tandem results and impact on processing and products. Mar Geodesie 34(3-4):214–241.

Drange H, Simonsen K (1996). Formulation of air-sea fluxes in the ESOP2 version of MICOM. Technical Report No. 125. Nansen Environmental and Remote Sensing Center.

Ducet N, Le Traon PYL, Reverdin G (2000). Global high-resolution mapping of ocean circulation from TOPEX/Poseidon and ERS-1 and -2. J Geophys Res 105:19,477–19,498.

Duncombe Rae, C.M, (1991). Agulhas Retroflection Rings in the South Atlantic Ocean: An Overview. South African Journal of Marine Science. 11, 327–344.

Duncombe Rae, C.M, Garzoli, S.L, Gordon, A.L, (1996). The eddy field of the southeast Atlantic Ocean: a statistical census from the Benguela Sources and Transports Project. Journal of Geophysical Research 101 (C5), 11,949–11,964.

Elaine L. McDonagh, Harry L. Bryden, Brian A. King, Richard J. Sanders (2008). The circulation of the Indian Ocean at 32°S, Progress in Oceanography, Volume 79, Issue 1, Pages 20-36.

Emery WJ, Meincke J (1986). Global water masses: Summary and review. Oceanol Acta 9(4).

Evensen G (2003). The Ensemble Kalman Filter: Theoretical formulation and practical implementation. Ocean Dyn 53:343–367.

Evensen G, van Leeuwen P (1996). Assimilation of Geosat altimeter data for the Agulhas Current using the Ensemble Kalman Filter with a quasi-geostrophic model. Mon Weather Rev 24:85–96.

Gaspari G, Cohn SE (1999). Construction of correlation functions in two and three dimensions. Q J R Meteorol Soc 125:723–757.

George MS, Bertino L, Johannessen OM, Samuelsen A (2010). Validation of a hybrid coordinate ocean model for the Indian Ocean. J Oper Oceanogr 3(2):25–38.

Goni G, Garzoli, S.L, Roubicek, A.J, Olson, D.B, Brown, O.B, (1997). Agulhas ring dynamics from TOPEX/POSEIDON satellite altimeter data. Journal of Marine Research 55, 861–883.

Goschem WS, Schumann EH (1990). Agulhas current variability and inshore structures off the Cape Province, South Africa. Journal of Geophysical Research, 95(C1), 667-678.

Grundlingh M.L, (1978). Drift of a satellite-tracked buoy in the Southern Agulhas Current and Agulhas Return Current. Deep Sea Research. 25, 1209–1224.

Grundlingh M. L, (1979). Observation of a large meander in the Agulhas Current. Journal of Geophysical Research, 84 (C7), 3776–3778.

Grundlingh M. L, (1980). On the volume transport of the Agulhas Current. Deep Sea Research, 27, 557-563.

Grundlingh M.L, (1983). On the course of the Agulhas Current. South African Geographic Journal. 65, 49–57.

Grundlingh M.L, (1992): Agulhas meanders: Review and a case study. South African Geographic Journal, 74, 19–28.

Hellerman S and Rosenstein M, (1983). Normal monthly wind stress over the world ocean with error estimates. Journal of Physical Oceanography, 13, 1093-1104.

Hoffman E.E, (1985). The large-scale horizontal structure of the Antarctic Circumpolar Current from FGGE drifters. Journal of Geophysical Research. 7, 245–270.

Kalman R.E. (1960). A new approach to linear filtering and prediction problems, Transactions of the ASME – Journal of Basic Engineering, Series D, 82, pp. 35–45.

Kara A, Rochford PA, Hurlburt HE (2000). Efficient and accurate bulk parameterizations of air-sea fluxes for use in general circulation models. J Atmos Ocean Technol 17:1421–1438.

Killworth PD, Dieterich C, Le Provost C, Oschlies A, Willebrand J (2001). Assimilation of altimetric data and mean sea surface height into an eddy-permitting model of the North Atlantic. Progress in Oceanography, Volume 48, Issues 2–3, Pages 313-335, ISSN 0079-6611.

Locarnini RA, Mishonov AV, Antonov JI, Boyer TP, Garcia HE (2006). World Ocean Atlas 2005, Volume 1: Temperature, p 182. NOAA Atlas NESDIS 61. U.S. Government Printing Office, Washington.

Lumpkin R, Pazos M (2007). Lagrangian Analysis and Prediction of Coastal and Ocean Dynamics (LAPCOD), chap. 2: Measuring surface currents with Surface Velocity Program drifters: the instrument, its data, and some recent results. Cambridge University Press.

Lutjeharms J.R.E, (1981a). Spatial Scales and intensities of circulation in the ocean areas adjacent to South Africa. Deep Sea Research, 28, 1289-1302.

Lutjeharms J.R.E, (1981b). Features of the southern Agulhas Current circulation from satellite remote sensing. South African Journal of Science. 77, 231-236.

Lutjeharms J.R.E, van Ballegooyen R.C, (1984). Topographic control in the Agulhas Current system. Deep Sea Research, 31, 1321-1337.

Lutjeharms J.R.E, Gordon, A.L, (1987). Shedding of an Agulhas Ring observed at sea. Nature 325, 138–140.

Lutjeharms J.R.E, Roberts H.R, (1988). The Natal Pulse: An extreme transient on the Agulhas Current. Journal of Geophysical Research. 93, 631–645.

Lutjeharms J.R.E, van Ballegooyen R.C, (1988a). The retroflection of the Agulhas Current. Journal of Physical Oceanography, 18, 1570-1583.

Lutjeharms J.R.E, van Ballegooyen R.C, (1988b). Anomalous upstream retroflection in the Agulhas Current. Science. 240, 1770–1772.

Lutjeharms J. R. E, Catzel R, Valentine, H.R (1989). Eddies and other border phenomena of the Agulhas Current. Continental Shelf Res. 9, 597–616.

Lutjeharms J.R.E, Weeks S.J, van Ballegooyen R.C, Shillington F.A, (1992). Shedding of an eddy from the seaward front of the Agulhas Current. South African Journal of Science. 88, 430–433.

Lutjeharms JRE, Webb DJ (1995). Modelling the Agulhas current system with FRAM (fine resolution antarctic model). Deep Sea Res. Part I 42:523–551.

Lutjeharms J.R.E, Cooper, J, (1996). Interbasin leakage through Agulhas filaments. Deep-Sea Res. 43, 213–238.

Lutjeharms J.R.E, (1996). The exchange of water between the South Indian Ocean and the South Atlantic. In: Wefer, G., Berger, W.H., Siedler, G., Webb, D.J. (Eds.), The South Atlantic: Present and Past Circulation. Springer, Berlin, Heidelberg, pp. 121–124.

Lutjeharms J.R.E, Ansorge, I, (2001). The Agulhas Return Current. Journal of Marine Systems 30, 115-138.

Lutjeharms J. R. E, Boebel O, Rossby T, (2003). Agulhas cyclones, Deep Sea Res. II, 50, 13–34.

Lutjeharms JRE (2006). The Agulhas Current. Springer-Praxis Books.

Lutjeharms J.R.E, (2007). Three decades of research on the greater Agulhas Current. Ocean Science. 3, 129–147.

Matano R.P, Simionato C.G, Ruijter W.P, van Leeuween P.J, Strub P.T, Chelton D.B, Schlax M.G, (1998). Seasonal variability in the Agulhas Retroflection region. Geophysical Research Letters, 25, 23, 4361-4364.

Meehl GA, Goddard L, Murphy J, Stouffer RJ, Boer G, Danabasoglu G, Dixon K, Giorgetta MA, Greene AM, Hawkins E, Hegerl G, Karoly D, Keenlyside N, Kimoto M, Kirtman B, Navarra A, Pulwarty R, Smith D, Stammer D, Stockdale T (2009). Decadal Prediction. Bull Amer Meteor Soc 90:14671485.

Oke P, Allen J,Miller R, Egbert G, Kosro P (2002). Assimilation of surface velocity data into a primitive equation coastal ocean model. J Geophys Res 107:511. doi:10.1029/2000JC000.

Oke P, Sakov P, Corney S (2007). Impacts of localisation in the EnKF and EnOI: Experiments with a small model. Ocean Dyn 57: 32–45.

Oke P, Schiller A, Griffin D, Brassington G (2005). Ensemble data assimilation for an eddy-resolving ocean model of the Australian Region. Q Jl R Met Soc 131:33013311.

Oke PR, Brassington GB, Griffin DA, Schiller A (2008). The Bluelink ocean data assimilation system (BODAS). Ocean Model 21: 46–70.

Oki T, Sud YC (1998). Design of the global river channel network for Total Runoff Integrating Pathways (TRIP). Earth Interactions 2(2-001):1–37.

Ollitrault M, Rannou J (2013). ANDRO: an Argo-based deep displacement dataset. J Atmos Ocean Technol 30(4):759–788.

Peeters FJC, Acheson R, Brummer GA, de Ruijter WPM, Schneider RR, Ganssen GM, Ufkes E, Kroon D (2004). Vigorous exchange between the Indian and Atlantic oceans at the end of the past five glacial periods. Nat 430:661–665.

Penven P, Chang N, Shillington F (2006). Modelling the Agulhas Current using SAfE (Southern Africa Experiment). In: Proc. EGU General Assembly. Vienna.

Penven P, Herbette S, Rouault M (2010). Ocean Modelling in the Agulhas Current System. In: Proceedings of the Joint Nansen-Tutu Scientific Opening Symposium and Ocean South Africa Meeting. Nansen-Tutu Centre for Marine Environmental Research.

Persistence Method: today equals tomorrow (2010). The Weather World 2010 Project, University of Illinois. http://ww2010.atmos.uiuc.edu/(Gh)/guides/mtr/fcst/mth/prst.rxml.

Quartly GD, Buck JJH, Srokosz MA, Coward AC (2006). Eddies around Madagascar — the retroflection re-considered. Journal of Marine Systems, Volume 63, Issues 3–4, Pages 115–129.

Rio MH, Guinehut S, Larnicol G (2011). New CNES-CLS09 global mean dynamic topography computed from the combination of GRACE data, altimetry, and *in situ* measurements. J Geophys Res 116:C07018. doi:10.1029/2010JC006505.

Rouault M, Penven P, Pohl B (2009). Warming in the Agulhas Current system since the 1980s. Geophys Res Lett L12:602.

Schiller R, Kourafalou V (2010). Modeling river plume dynamics with the Hybrid Coordinate Ocean Model. Ocean Model. doi:10.1016/j.ocemod.2009.12.005.

Schouten M.W, de Ruijter W.P.M, van Leeuwen P. J, (2002). Upstream control of Agulhas ring shedding. Journal of Geophysical Research. 107, doi:10.1029/2001JC000804.

Shottle S, (2002). The Impact of Sea Surface Height Data Assimilation on El Nino Analyses and Forecast. Max-Plank Institute for Meteorology. Dissertation for Doctorate, University of Hamburg. ISSN 0938-5177.

Srinivasan A, Chassignet E, Bertino L, Brankart J, Brasseur P, Chin T, Counillon F, Cummings J, Mariano A, Smedstad O, Thacker W (2011). A comparison of sequential assimilation schemes for ocean prediction with the HYbrid Coordinate Ocean Model (HYCOM): Twin experiments with static forecast error covariances. Ocean Mod 37:85–111.

Steele M, Morley R, Ermold W (2001). PHC: a global ocean hydrography with a high quality Arctic Ocean. J Clim 14:2079–2087.

Thoppil PG, Richman JG, Hogan PJ (2011). Energetics of a global ocean circulation model compared to observations. Geophys Res Lett 38. doi:10.1029/2011GL048347.

Toole J and Raymer M, (1985). Heat and flesh water budgets of the Indian Ocean-revisited. Deep Sea Research. 32,917-928.

van Ballegooyen R.C, Grundlingh, M.L, Lutjeharms, J.R.E, (1994). Eddy fluxes of heat and salt from the southwest Indian Ocean into the southeast Atlantic Ocean: a case study. Journal of Geophysical Research. 99, 14053–14070.

van Leeuwen P. J, De Ruijter W.P.M, and Lutjeharms J.R.E, (1999). Natal Pulses and the formation of Agulhas rings. Journal of Geophysical Research. in press.

van Sebille E, Biastoch A, van Leeuwen PJ, de Ruijter WPM, (2009). A weaker Agulhas Current leads to more Agulhas leakage. Geophys Res Lett 36. doi:10.1029/2008GL036614.

Wallcraft AJ,Metzger EJ, Carroll SN, (2009). Software Design Description for the HYbrid Coordinate Ocean Model (HYCOM) Version 2.2. Technical Report NRL/MR/7320–09-9166. Naval Research Laboratory.

Wunsch C, Stammer D, (1998). Satellite altimetry, the marine geoid, and the oceanic circulation. Annu Rev Earth Planet Sci 26:219–253.

Wyrtki K, (1971). Oceanographic Atlas of the International Indian Ocean Expedition. National Science Foundation, Washington, D.C, 531 pp.

Xie J, Counillon F, Zhu J, Bertino L, (2011). An eddy resolving tidaldriven model of the South China Sea assimilating along-track SLA data using the EnOI. Ocean Sci 7:609–627.